THE INVESTIGATION OF MICROLAYER GEOMETRY DURING NUCLEATE BOILING ON A FLAT PLATE

By

HARVEY PARNELL METZLER

Bachelor of Science
University of Kansas
Lawrence, Kansas
1963

Master of Science
University of Kansas
Lawrence, Kansas
1967

Submitted to the faculty of the Graduate College of
the Oklahoma State University
in partial fulfillment of the requirements
for the degree of
DOCTOR OF PHILOSOPHY
May, 1970

THE INVESTIGATION OF MICROLAYER GEOMETRY

DURING NUCLEATE BOILING

ON A FLAT PLATE

Thesis Approved:

Jerald D. Parker
Thesis Adviser

J. A. Clubb

Lloyd Lister

R. L. Lowery

D. Durham
Dean of the Graduate College

ACKNOWLEDGMENTS

During the course of this three-year endeavor, I have had the assistance of many individuals. As a small formal token of my true appreciation, I would like now to acknowledge this help.

I would first like to thank Dr. J. D. Parker, Dr. H. T. Fristoe, Dr. R. L. Lowery, and Dr. J. A. Wiebelt for serving on my graduate committee.

Since my experimental work was only partially sponsored, I found it necessary to design and build the specialized hardware needed for the investigation. I am very grateful to the many people who gave me their professional as well as personal time to help me locate raw materials and advise me on design and manufacturing problems. Without this help, my research would have been an economic impossibility.

From O.S.U., the list includes: M. Wayne Adkins, Merritt R. Ashcraft, Kenneth J. Bell, C. R. Brewer and staff, Maurice L. Colpitts, George M. Cooper, Robert D. Freeman, Harold T. Fristoe, Heinz Hall, Arlin L. Harris, William L. Hughes, Daniel D. Lingelbach, Eugene E. McCroskey, Charles M. Stockwell, Gerald H. Stotts, Harry G. Wallace, Preston G. Wilson, and Peter R. Worch.

From outside O.S.U., the list includes: Jack H. Adams, Eagle Pitcher Industries; Elmer A. Allen, Triangle A&E; W. E. Beckner, Corning Glass; John P. Ford, Sandia Laboratories; George S. Freeman, Fenwal Electronics; Morgan Hunter, Labglass; W. H. Kroeck, Bell Telephone Laboratories, R. D. Mathis, R. D. Mathis Company;

Orville (Mike) Mauck, ARCO; Russell B. Mesler, University of Kansas; Hans Mroch, Tibon Plating; Robert L. Owens, California Computing Company; Neith J. Pollard, Sandia Laboratories; John E. Schwenker, Bell Telephone Laboratories; Thomas R. Smith, Lew Wenzel & Company; and Jimmie L. Stewart, Applied Science Associates.

I had excellent cooperation from dozens of technical representatives in industry in solving material and hardware problems. Their assistance and donations were appreciated.

A special thank you is extended to Robert E. Cunningham and Norman L. Freeman for their professional help and friendship through the many lows when the research goals looked unattainable.

I would like to thank Eldon Hardy and Professor Lora Todd for their excellent assistance in preparing the manuscript.

The Electrical and Chemical Engineering Departments donated the use of many thousands of dollars worth of equipment to the project. Their unselfishness in sharing research tools across departmental boundaries is greatly appreciated.

NASA provided me with a traineeship that partially paid for my living expenses and bought some supplies. Their financial assistance is acknowledged.

I want to thank my parents and my wife's parents for their patience, encouragement and understanding during a very trying period of my life.

Last and most, I want to thank my wife, Claudette, for her countless contributions to the dissertation. Without her professional help in writing my computer programs, being my full time lab assistant and editing and typing the manuscript, the time required for me to complete

the dissertation would have been prohibitive. Without her moral support, I could not have mentally endured the many thousands of hours of frustration and failure experienced to bring the dissertation to a successful completion.

The dissertation is dedicated to the memory of the late Dr. and Mrs. J. T. Swanson.

TABLE OF CONTENTS

LIST OF FIGURES

NOMENCLATURE

B_ℓ	bubble lifetime
C_i	specific heat of node i
C_p	specific heat of liquid or liquid microlayer
CAP_i	thermal capacity of node i
dh	differential enthalpy on unit mass basis
du	differential internal energy of system on unit mass basis
dv	differential specific volume
$d\delta$	differential microlayer thickness
$d\theta$	differential time
h_1	enthalpy of microlayer at instant evaporation begins on unit mass basis
h_2	enthalpy of saturated liquid on unit mass basis
h_3	enthalpy of saturated vapor on unit mass basis
h_{fg}	enthalpy of vaporization on unit mass basis
i	matrix subscript
j	matrix subscript
${}_jA_i$	perpendicular area associated with heat flow from node j to node i
${}_jCON_i$	thermal conductance from node j to node i
${}_jK_i$	thermal conductivity of material between node j and node i
${}_jL_i$	distance between node j and node i
K	thermal conductivity
$K_{m\ell}$	thermal conductivity of microlayer

L	fixed distance along z axis at which temperature in solid is known
P	pressure
$q''_{1,j}$	heat flux from node j below surface to node 1 on surface
$q''(\theta)$	instantaneous heat flux beneath microlayer
q_i''	initial heat flux to microlayer at instant vaporization begins
Q	heat transfer per bubble
r	bubble radius or distance along r axis
R	maximum bubble radius
R_d	dry radius in meters
$\overline{R}$	maximum distance that temperature disturbance propagates in radial direction
S	entropy
t	time from nucleation in hours
t_g	time taken for the bubble to grow to the point considered
T	temperature
T_i	temperature at node i
$T_{i,j}$	temperature at node i,j
$T_{i,m}$	temperature at node i at the present time
$T_{i,m+\Delta\theta}$	temperature at node i one time step in the future
T_j	temperature at node j
$T_{j,m+\Delta\theta}$	temperature at node j one time step in the future
T_1	average temperature of microlayer at instant vaporization begins
T_2	temperature of saturated liquid
T_b	liquid bulk temperature
T_{hs}	heater surface temperature
T_{ia}	average microlayer temperature at beginning of vaporization

T_{ihs} heater surface temperature beneath microlayer at instant vaporization begins

T_s saturation temperature

V_i volume of node i

z distance along z axis

GREEK

α thermal diffusivity of fluid

δ instantaneous microlayer thickness

δ_i initial microlayer thickness

δq differential of heat transfer to or from system on unit mass basis

δw differential of work to or from system on unit mass basis

ΔT temperature difference

ΔT_i change in temperature at node i in one time step ($\Delta\theta$)

Δx spatial distance associated with temperature difference (ΔT)

$\Delta\theta$ time step

θ time, the independent variable

ν kinematic viscosity

ρ_i density of node i

ρ_ℓ liquid density

$\rho_{m\ell}$ density of microlayer

τ time for microlayer at any particular radius to evaporate to dryness

CHAPTER I

INTRODUCTION

Nucleate boiling is a mode of heat transfer that has caused a great deal of confusion in heat transfer literature during the past two decades. As experimental evidence has been gathered, many models have been proposed to explain the data. Three models dominate the literature.

In 1960 Rohsenow and Clark [23]* postulated that the high heat flux encountered in boiling was the result of vapor bubbles acting as fluid agitators and fluid pumps in the vicinity of the heat transfer surface. Agitation took place as expanding bubbles pushed back the surrounding fluid, Figure 1 (a). Pumping action took place when the bubbles buoyantly lifted from the heat transfer surface and were replaced by inrushing fluid, Figure 1 (b). With respect to a bubble, the path of heat transfer was from the heated plate to the surrounding fluid and finally through the bubble wall. This particular model was so qualitative that it was impossible to distinguish between surface and bubble exchange and surface and liquid exchange. However, it became quite popular in the literature until it was recognized that the model failed to account for the insensitivity of nucleate boiling heat flux to subcooling.

---

*Numbers in brackets designate References listed in List of References.

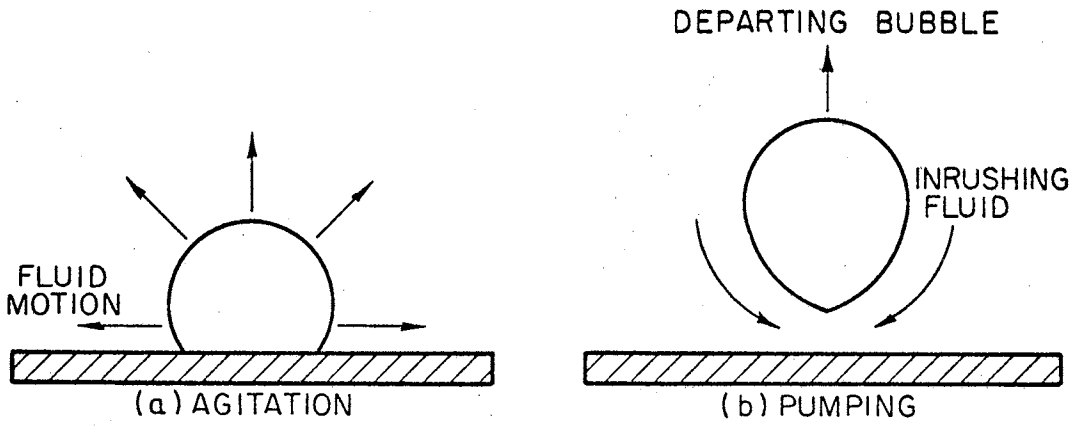

Figure 1. Rohsenow-Clark Model

In subcooled boiling, the bulk fluid temperature is below the saturation temperature for a particular pressure. According to the Rohsenow-Clark model, a cooler bulk fluid, when mixed with the hot fluid layer next to the heating surface, should have promoted heat transfer. Since this was contrary to fact, another model proposed by Forster and Grief [7] was adopted.

In the Forster-Grief model a bubble forms at a nucleation site on the heat transfer surface beneath the thermal layer. The thermal layer is a thin liquid layer next to the heat transfer surface through which

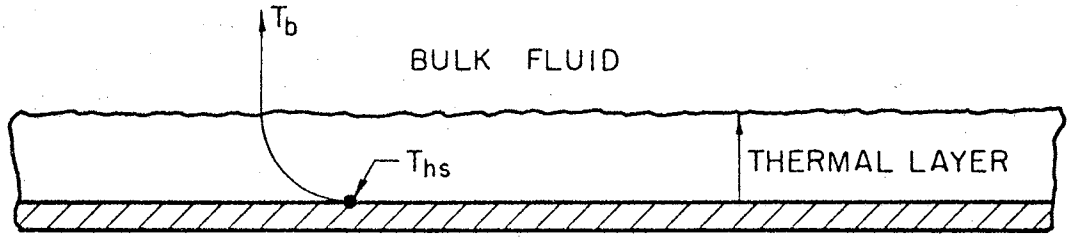

Figure 2. Thermal Layer

the temperature drops from the heater surface temperature T_{hs} to the bulk fluid temperature T_b, Figure 2. Heat flows from the heater surface into the thermal layer and finally passes through the bubble wall causing the bubble to grow. As the bubble grows, it pushes a portion of the thermal layer out into the bulk fluid, Figure 3. When the bubble breaks away from the surface and rises into the fluid, it carries

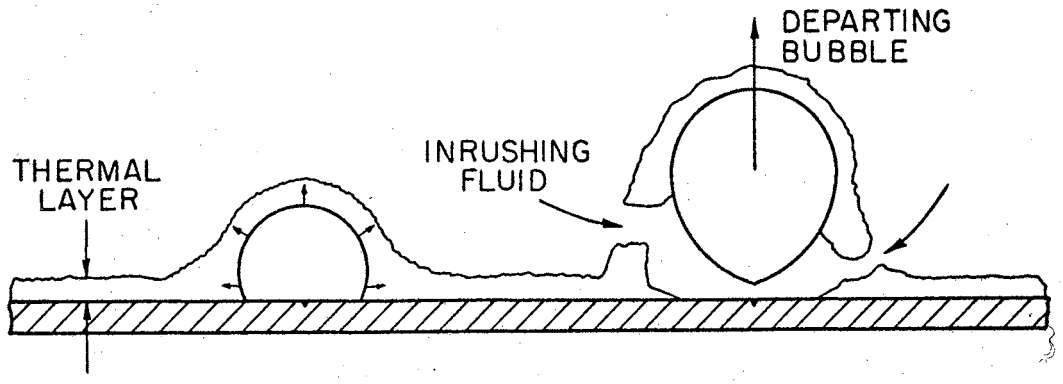

Figure 3. Forster-Grief Model

a portion of the thermal layer with it. The void left by the departing bubble is refilled by inrushing cool liquid. Thus, the growing bubbles are continually replaced with cool fluid as they 'pump' portions of the thermal layer out into the fluid bulk.

Forster and Grief explained the insensitiveness of boiling heat flux to subcooling from a thermal layer consideration. They stated that it makes no difference on the heat transfer whether a bubble rises into saturated liquid or grows into subcooled liquid and collapses; the same volume of thermal layer is forced into the fluid bulk in either

case if the maximum bubble diameter is the same. They further stated that:

$$Q \sim C_p \rho_\ell R^3 (T_{hs} - T_b) \frac{1}{B_\ell} . \qquad (1\text{-}1)$$

With increased subcooling, T_b is lowered and B_ℓ decreases making $(T_{hs} - T_b) \frac{1}{B_\ell}$ larger. However, R^3 decreases and cancels the increase in the other terms, so the net effect of subcooling is negligible.

The Forster-Grief model was commonly accepted until Snyder [25] postulated that perhaps evaporation from a thin fluid layer at the bubble base with simultaneous condensation on the bubble dome could account for boiling heat flux. Snyder thought that precise temperature measurements at the bubble base during growth would prove his hypothesis but he was unable to make such measurements. However, by following Snyder's premise, other investigators were successful, and a third model for boiling began to appear in the literature.

CHAPTER II

LITERATURE REVIEW

A review of the recent literature which has evolved from Snyder's [25] evaporation-condensation hypothesis for bubble growth is focused on experimental investigations to obtain information about evaporation at the bubble base or condensation on the bubble dome. Temperature measurements and photographic observations have disclosed the existence of evaporation at the bubble base.

Evaporation at the Bubble Base

Moore and Mesler [21] used a tiny, fast response thermocouple to measure the surface temperature at one location on a thin Nichrome V strip. The thermocouple was formed by placing an insulated Alumel wire in a Chromel P tube. Water was boiled on the Nichrome V strip at atmospheric conditions and with heat fluxes ranging from 135,000 to 202,000 Btu per hour per square foot. Temperature excursions of 20°F to 30°F which took place in two milliseconds were observed. Such rapid heat extraction was not compatible with the agitation models. When conduction theory was applied to the heater element by treating it as a semi-infinite solid, the authors found that water 147°F cooler than the heater surface would have to be brought in contact with it to cause the experimental temperature drops. Since such a cold fluid does not exist in boiling, the quenching mechanism at bubble departure

hypothesized by earlier investigators was ruled out. The authors proposed that a thin liquid layer called the microlayer must form beneath the bubble and evaporate into its interior. The evaporation was thought to occur with simultaneous condensation on the bubble dome. This form of microlayer mass transfer seemed the only plausible explanation to account for the rapid temperature drops. The microlayer was estimated to range in thickness from 78 to 89 microinches and to account for 70 to 90 percent of the total heat flux.

Rogers and Mesler [22] used a thermocouple in conjunction with an artificial nucleation site and high-speed photography to study surface temperature fluctuations and relate them to bubble growth. The thermocouple was similar to that used by Moore and Mesler [21]. The artificial nucleation site, at the center of the Alumel wire, was formed by pricking with a sharp needle. The thermocouple's tiny junction was formed by either pricking the Alumel wire over into the Chromel P tube with a needle or by vapor plating a 0.002 inch arc of the Chromel P annulus. Water was boiled on a Chromel P strip which was resistance heated. Heat flux was varied from 19,000 to 51,000 Btu per hour per square foot. The temperature at the artificial site was observed to drop as the bubble grew. No significant cooling was apparent when the bubble departed from the surface and was replaced by inrushing fluid. This contradicted the quenching model hypothesized by earlier investigators.

Hendricks and Sharp [9] studied boiling of subcooled water from Nichrome ribbons which were resistance heated. Temperatures were read with three tiny thermocouples silver-soldered to the heater subsurface. High-speed pictures were synchronized to the thermocouple readout. The

same happenings were observed at a thermocouple located slightly less than one bubble diameter from the nucleation site as were observed at a thermocouple located slightly greater than one bubble radius from the site. No appreciable effect on heat transfer was seen during growth, and there was only a small rise in the heat flux during collapse. These observations ruled out microconvection or turbulence in the thermal layer as a major mode of heat transfer in boiling. For the third thermocouple, located slightly less than one bubble radius from the nucleation site, a rapid temperature drop was observed as soon as the bubble base perimeter passed over the thermocouple; the temperature drop was accompanied by a twenty-fold increase in the average heat flux beneath the bubble. For the thermocouple located under the bubble, an appreciable decrease in heat flux was noticed during bubble collapse. Over this thermocouple the heat flux at times even went negative, indicating that the thermal layer was hotter than the plate under the bubble once microlayer evaporation had occurred. This negative flux was probably the result of the low heat capacity of the thin ribbon heater coupled with an extraction of heat at a faster rate than could be generated internally. A rough calculation estimated microlayer thickness at 32 microinches.

Madsen [17] conducted two different experiments on the nucleate boiling of water at various pressures. In the first experiment, the boiling surfaces, which were nickel-plated stainless steel or nickel-plated copper, were heated by a copper block cast around an embedded resistance heater. Surface temperatures were recorded by small copper-constantan thermocouples. Temperature fluctuations similar in magnitude but different in shape from those reported by Moore and

Mesler [21] were reported by Madsen. An increase in pressure had the effect of increasing the frequency of the temperature drops while decreasing their amplitude. Madsen seemed unclear as to whether the shape of the temperature excursions was a true indication of the heater surface temperature or whether the shape was greatly distorted because of his thermocouple geometry.

Cooper and Lloyd [4] boiled toluene at reduced pressures on heated pyrex. Surface temperatures under individual bubbles were measured with four vacuum deposited film thermometers. A temperature drop similar to that reported by other investigators was observed as the bubble perimeter passed over each thermometer. By coupling a first law analysis with a conduction solution of the heat flow through the pyrex during bubble growth, an estimate was made of the thickness of the microlayer at the instant it was left behind by the bubble perimeter to begin its evaporation. Cooper and Lloyd concluded:

1. A change in heat flux has very little effect on the formation of the microlayer.
2. If metallic heaters were used rather than pyrex, they would not experience so large a surface temperature drop beneath each bubble because heat would flow from the underlying metal almost as fast as it could be extracted by the evaporating microlayer.
3. No increase in heat flux was noticed beyond the maximum bubble radius.

In a recent paper, Cooper and Lloyd [5] coupled the experimental work of [4] to a simplified hydrodynamic model. The resulting equation from the hydrodynamic considerations for initial microlayer thickness

was:

$$\delta_i = 0.8\sqrt{\nu\, t_g} \,. \qquad (2\text{-}1)$$

Equation (2-1) made possible the calculation of the total volume of vapor that evaporated from the microlayer into a bubble. Calculated volumes were compared to experimental volumes taken from high-speed motion pictures of the bubble profile for one saturated and one subcooled case. Agreement between the two volumes was good for the saturated case, but, under subcooled conditions, the calculated volume was much larger than the experimental volume. This discrepancy between the two volumes for the subcooled case was attributed to vapor condensation on the bubble wall during growth.

Hospeti [10] boiled water at atmospheric conditions on a thin Chromel P strip in which a small Chromel-Alumel thermocouple was embedded for recording the surface temperature fluctuations. A dual-lens high-speed camera was used to record simultaneously the bubble profile and the temperature trace displayed on an oscilloscope. In one case data was taken with the thermocouple finished identically with the rest of the boiling surface, while in a second case, a small artificial cavity was formed at the thermocouple junction.

A comparison was made between microlayer vaporization and total latent heat contained in the bubbles either at their maximum contact diameter or at detachment. Latent heat content was determined from volume calculations made from the camera film. Microlayer vaporization contributions were estimated by calculating the heat removed from the surface of a semi-infinite solid undergoing the same surface temperature fluctuations as the boiling surface. An estimate of the

contribution of microlayer vaporization to total heat flux as a function of heat flux was made with the artificial site.

Microlayer vaporization was found to account for 1.5 percent to 100 percent of the bubble latent heat content at departure. The contribution of microlayer vaporization to total heat flux decreased with increasing heat flux. Hospeti proposed that the nucleation characteristics of the artificial site could have changed with increasing heat fluxes and led to the conclusion that microlayer vaporization became less important at higher heat fluxes.

McSweeney [20] boiled toluene and ethyl alcohol on soda lime glass at a local hot spot heated by a tiny cartridge heater. Temperatures were measured on the boiling surface by six vacuum deposited nickel resistors, two of which were monitored at any one time by an oscilloscope. The nickel resistors measured an average temperature over a rectangular surface area approximately 0.020 inches by 0.026 inches. Still photographs were taken during bubble growth from the top and front of the boiler by using two cameras simultaneously. Attempts at controlling nucleation were made with teflon as an artificial site.

For both toluene and ethyl alcohol, the bubble growth rate increased inversely with pressure. Ethyl alcohol exhibited nucleation from both natural and artificial sites while toluene only nucleated at the artificial site. Once boiling began, the toluene and alcohol exhibited different characteristics. Toluene nucleated many bubbles in quick succession followed by a waiting period. For toluene, the microlayer vaporized rapidly leaving the surface insulated for considerable time before lift-off. Once lift-off occurred, the surface recovered to instantaneously nucleate another bubble. Microlayer vaporization for

the alcohol was more gradual; the surface did not have time to recover before lift-off, and a waiting period was, therefore, necessary to reform the microlayer. For the ethyl alcohol, only about three percent of the total heat and 30 percent of the bubble latent heat at lift-off could be attributed to bubble-induced agitation and conduction across the thermal layer. The author hypothesized that even though the microlayer vaporization accounted for only a small part of the total heat transfer, it still controlled nucleation and, therefore, governed boiling heat transfer.

Hospeti and Mesler [11] studied boiling on a Chromel P strip in a calcium sulfate solution containing radioactive Sulfur 35. Bubble growth was recorded with a high-speed camera. Calcium sulfate was selected because it has a negative solubility slope, and deposits left behind by an evaporating fluid layer would not go back into solution when the surface was again flooded at bubble departure. Autoradiographs of the deposits examined with a densitometer indicated that the microlayer that evaporated was uniform in thickness since it left behind uniform deposits. A Geiger counter reading of each deposit was used to estimate the quantity of sulfate deposited. By knowing the quantity of sulfate, the strength of the original sulfate solution, the number of bubbles that it took to form the deposit, and the bubble contact diameter, it was possible to determine roughly the thickness of the microlayers that evaporated and left behind the sulfate deposits. Microlayer thicknesses between 46 and 103 microinches were reported.

Sharp [24] described two optical techniques that he used to successfully photograph a vaporizing microlayer and estimate its radial thickness as a function of time.

In one experiment Sharp directed a collimated beam of white light onto the underneath side of a piece of heated flint glass on which a bubble was growing in methanol. The reflected beam was photographed by a high-speed camera. When bulk liquid covered the flint glass, 0.354 percent of the incident light was reflected to the camera. When a microlayer was present, a double reflection occurred, and 0.696 percent of the incident light struck the camera. By this means, the base of the growing bubble was clearly defined, and the microlayer was found occasionally to evaporate to dryness at its center.

In a second experiment Sharp used interference techniques to determine microlayer thickness by directing light down through the top of a growing bubble while photographing the light as it reflected off the microlayer. The resulting interference pattern of light and dark rings when correlated to thicknesses indicated that the microlayer was radially symmetric and of increasing thickness from its center to the bubble perimeter. This was explained by pointing out that the perimeter had undergone less evaporation than the center due to its having been exposed to the bubble interior for a shorter time. The conclusions reached were:

1. The tendency for complete evaporation at the bubble base increased with heat flux.
2. The degree of drying was hypothesized to depend chiefly on the heater surface temperature at the time of nucleation and the conductivity of the heater surface.
3. The sharp boundary of the dry center indicated a definite contact angle.

4. Above certain heat fluxes, complete flooding of the dry center did not occur and bubbles grew from pulsating microlayers with initially dry centers.

Katto and Yokoya [15] studied boiling on a flat copper heater above which was mounted an interference plate that could be set at different heights above the heater surface. Water at atmospheric conditions was boiled while high-speed photographs were taken as the bubbles grew up and flattened themselves against the interference plate. A microlayer that evaporated to dryness in the center was observed at the base of the flattened bubbles. The radial velocity of the evaporation to dryness was found to be much slower than the bubble radial velocity. The dry radius was found to be a linear function of time. By coupling the photographic measurements with an analytical model, estimates were obtained of the thickness of the microlayer at the instant it was formed by the bubble perimeter as well as thicknesses during evaporation. Both thicknesses were thought to vary with the square root of bubble radius. The microlayer vaporization accounted for 67 percent of the total heat flux.

Kirby and Westwater [16] boiled carbon tetrachloride and methanol on a ground glass surface. The solid-liquid interface was coated with a transparent, electrically-conducting material heated by direct current. The liquids were boiled at atmospheric conditions while motion picture data was taken through the coated glass.

Latent heat transport by bubbles as they left the heater surface accounted for approximately nine percent of the total heat flux. Coalescence of bubbles into an overlying, irregular vapor mass was sometimes followed by the appearance of dry spots on the heater surface.

The dry spots were observed to increase in size and coalesce with surrounding dry spots. The state of the entire surface evaporating to dryness was hypothesized to be the time of transition from nucleate to film boiling.

Torikai [28] boiled water at atmospheric pressure on an electroconductive glass plate while photographically observing the bubble base through the glass. The photographs of the bubble base were typified by a dark center surrounded by a clear white outer torus. The dark center and white torus were indicative of dryness and wetness in the contact area. The dry center was observed to increase in diameter as the bubble grew. At high heat fluxes the evaporating liquid layer was thought to be responsible for most of the heat transfer.

Torikai and Yamazaki [29] performed two experiments of boiling on electroconductive glass with simultaneous high-speed photography of the bubble contact area taken through the glass. One study was of pool boiling on two different horizontal surfaces; one surface was bare while the second was coated with silicone. At low superheats, heat transfer from the coated surface was better than the bare surface while at higher superheats, the reverse was true. Burnout for the coated surface was one third of that for the bare surface. The high-speed photographs disclosed that the liquid did not wet the coated surface and bubbles formed on it with no microlayer in the contact area. However, microlayers were observed on the bare surface. The ratio of the contact area to the total area was greater for the silicone coated surface clear to burnout; at burnout this ratio became the same. At burnout no microlayers were present on either surface; flooding no longer had time to occur on the bare surface.

In a second study, the authors circulated water vertically through a rectangular flow channel, two sides of which were bare electroconductive glass. The high-speed photographs disclosed that the contact area in forced circulation was similar in shape to that found in pool boiling. However, such was not true of the bubble profiles as they were distorted from their hemispherical shape when they grew out into the boundary layer. The ratio of the contact area to total surface area was found to be similar for both forced circulation and pool boiling conditions at saturation. However, with subcooling, the ratio was smaller for forced circulation than for pool conditions.

In another study by Torikai and Yamazaki [30], water was boiled on one horizontal and one vertical surface of electroconductive glass while photographs were taken of the bubble base through the glass. Boiling studies were made under both saturated and subcooled conditions. Special emphasis was placed on obtaining information about the dry radius phenomena that occurs from evaporation to dryness of the thin liquid layer in the center of the bubble base.

A dark center with a surrounding light torus was observed during the later stages of bubble growth indicating a dry region with a surrounding wet periphery. The evaporation to dryness was not observed until after the fast growth period. Several bubbles evaporated to complete dryness in their contact area. The radial growth of the dry center was found to be independent of subcooling. Only ten percent of the total surface area was occupied by dry centers at any one time and this ten percent seemed to remain constant until approaching burnout.

Jawurek [14] boiled methanol and ethanol on Electropane at heat fluxes ranging from 10,000 to 30,000 Btu per hour per square foot and

at pressures from 0.2 to 0.5 atmospheres. Profile photographs of a growing bubble with interference photographs taken beneath the bubble were simultaneously recorded on the same film through a system of optics.

A wedge-shaped microlayer profile was observed which evaporated to dryness at its center and increased in thickness with time at the large radii. Microlayer thicknesses at the outer radii ranged from 0.2 to 0.8 microns.

Condensation at the Bubble Dome

Bankoff and Mason [3] measured heat transfer coefficients for the surface of single bubbles formed by injecting steam through hypodermic needles into a subcooled water stream at atmospheric pressure. Steam flow rates from 0.4 to 1.5 gal/min with water temperatures from 80°F to 180°F and water velocities from 0.9 to 7.2 ft/sec were used. The inlet for the cooling water was positioned above the steam injection chamber so that the water stream impinged on the bubble dome before flowing around the bubble periphery and out of the chamber. Bubbles were generated at rates between 200 and 2,500 per second. Bubble surface heat transfer coefficients between 13,000 and 320,000 Btu per hour per square foot were reported. The authors concluded that latent heat transport must be an important mechanism in nucleate boiling.

Bankoff [2] stated that a no-slip condition at the boiling surface would naturally keep liquid from being directly displaced from a solid as a nucleate boiling bubble expands. Therefore, a thin superheated microlayer was left behind by the bubble wall. It evaporated into the bubble interior with simultaneous condensation on the bubble dome. The

dome temperature was hypothesized to be considerably less than saturation to supply the driving force for the condensation. A simple one-dimensional calculation was made which indicated that latent heat transport, by simultaneous evaporation and condensation, could account for the major portion of the total heat flux near burnout.

Snyder and Robin [26] studied a bubble generated on the bottom of a square cross-section flow channel while subcooled water was flowing down the channel. The purpose of this investigation was to substantiate the idea that sufficient condensation rates at the bubble cap were present to support the microlayer vaporization model. This model had been hypothesized by Snyder in 1956 [25] to include vaporization from a thin fluid layer at the bubble base with simultaneous condensation taking place at the bubble dome. The bubbles studied in the current experiment were generated by injecting steam through a tiny hole in a heated stainless steel plate at the channel base. The bubbles grew from the small hole into the fluid stream whose velocity could be varied up to 40 ft/sec while the temperature was regulated from 80°F to 140°F. When the stainless plate was heated electrically, a thermal boundary layer, independent of the steam injection rate, was established.

The condensation rates observed proved that indeed a large amount of heat could be removed from the bubble dome during subcooled boiling. Mass transfer was felt to be the predominant heat transfer mechanism in subcooled nucleate boiling. The thickness of the thermal layer was found to have no effect on the condensation rates. This finding was in direct conflict with the old thermal layer pumping model of Forster and Grief [7].

Jacobs and Shade [13] studied the boiling of carbon tetrachloride at atmospheric pressure from a platinum strip heater. Temperature measurements were made with a single thermocouple probe that could be micrometer positioned at any point above the heat transfer surface. Photographic data was taken with a high-speed camera and a Schlieren optical system. Data was taken from the natural convection stage up to burnout.

When the thermocouple probe was located between active sites, little temperature excursion was noted. The data was characterized by a rapid rise in temperature as the probe pierced a bubble. Once the probe was inside the bubble, the temperature remained fairly stable. Then, as the bubble lifted from the heated surface and moved past the probe, gradually reduced temperatures were recorded in the bubble wake. The photographs indicated that the rising bubbles carried a thin cap of hot liquid on their upper dome and trailed a long, usually turbulent wake.

A General Model

Graham and Hendricks [8] developed a general model for nucleate boiling heat transfer. The model proposed time and surface area averages of the following basic heat transfer mechanisms:

1. Transient thermal conduction through the liquid thermal layer in the vicinity of a nucleation site that is preparing to bear a bubble.
2. Evaporation from a microlayer surface underneath a bubble that is attached to the heater surface.

3. Turbulent free convection that is taking place over the surface areas not covered by bubbles (a zone of enhanced convection occurs in the vicinity of a growing bubble).

By using the model conjunctively with experimental data on water and methanol, a comparison was made between the various mechanisms.

The conclusions reached were that no one single mechanism dominates over the entire range of heat flux. Evaporation was found to be the major contributor to fluxes greater than 20 percent of critical. Transient conduction through the thermal layer was found to rank next in importance, with convection being last. A great deal of good data on contact area, evaporative-condensing processes and thermal diffusion into the liquid bulk was found to be lacking in the literature and was needed for application of the model.

CHAPTER III

MICROLAYER GEOMETRY--PAST AND PROPOSED

Microlayer vaporization with simultaneous condensation has been shown to exist. Although the quantitative information is still rather controversial, the fact remains that an evaporating microlayer plays a major role in nucleate boiling heat transfer.

The Microlayer

The phenomena of the evaporating microlayer can best be understood by an examination of a nucleation site on the heat transfer surface; this site will be a localized hot spot, pit, scratch, or some other type of surface imperfection.

A bubble will form and grow, as illustrated in Figure 4, from a small vapor nucleus at the nucleation site. As it grows radially, the bubble perimeter leaves behind a thin liquid layer beneath the bubble, commonly called the microlayer. This is a continuing process as the bubble perimeter expands from 0 to A and on to B. As the microlayer is formed, heat is immediately conducted into it from the heated solid causing it to begin evaporation into the bubble interior. Part of the vapor from the evaporating microlayer condenses on the cool bubble dome since the dome acts as a boundary of heat exchange between the bubble interior and the surrounding bulk fluid. The portion of the vapor from the microlayer that does not condense is carried away as latent heat by

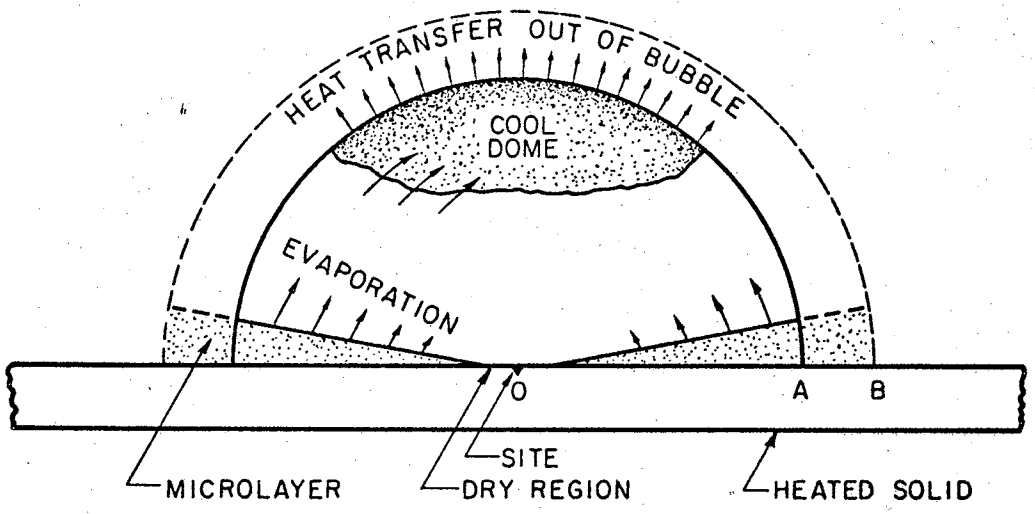

Figure 4. Expanding Bubble with Microlayer Evaporation

the bubble at lift-off.[1] At lift-off it is quite common for microlayer vaporization to have proceeded to dryness over a sizeable portion of the contact area.

During microlayer vaporization, there are two thicknesses of interest, an initial thickness and an instantaneous thickness. The initial microlayer thickness (δ_i) is the thickness of the thin fluid layer at the bubble perimeter at the moment evaporation begins. The instantaneous microlayer thickness (δ) is the thickness of the microlayer at any radius between the expanding perimeter and bubble center after evaporation commences. The definition of these two thicknesses

---

[1]Note that not all of the bubble latent heat has to originate with microlayer vaporization as it is also possible for evaporation to occur from the bubble sidewall. However, the problem of determining the exact portion of the sidewall that is engaged in evaporation or condensation at any instant has not been solved as it is a complex process taking place at a moving boundary inaccessible to direct measurement.

is best illustrated by the examination of the thin fluid layer beneath a bubble as the bubble grows over a sensitive thermocouple attached to the boiling surface, as shown by Figure 5. As the bubble perimeter

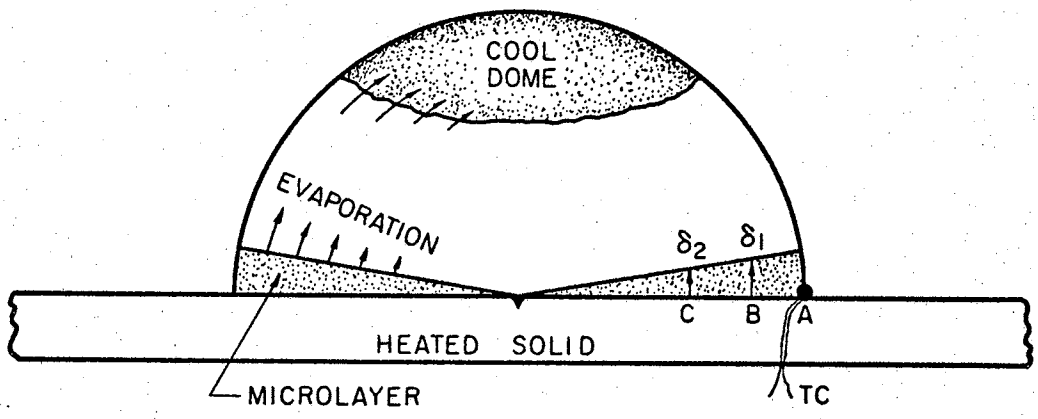

Figure 5. Microlayer Thicknesses

passes over the thermocouple located at A, the thermocouple will experience a temperature drop. At the moment that the drop commences, the initial microlayer thickness (δ_i) is the thickness of the fluid layer between the thermocouple and the vapor in the bubble interior. At this moment in time, the instantaneous microlayer thicknesses (δ's) are the thicknesses of the fluid layer at any radial position between the bubble perimeter and the bubble center, i.e., δ at B would be δ_1 and at C would be δ_2, etc.

Present State of the Art

Only limited information on microlayer thickness is reported in the literature. Most of the investigators considering thickness have at best made rough estimates of an average value based on a maximum bubble diameter or contact diameter. However, there are a few exceptions where thickness has been considered a function of radial position or a function of time or both.

Cooper and Lloyd [4] [5] estimated initial microlayer thickness (δ_i) at four radial positions beneath single bubbles. A plot of their results is shown in Figure 6. Note that there seems to be no strong indication that δ_i is a linear or nonlinear function of bubble radius as both trends are in evidence.

Sharp [24] made rough optical measurements of instantaneous microlayer thickness (δ) using interference techniques. A plot of his results is shown in Figure 7. The plot is indicative of a linear relationship between δ and bubble radius. The expanding dry radius phenomenon is also evident.

Katto and Yokoya [15] observed the expanding dry radius at the base of bubbles growing up against an interference plate. The dry radius was found to expand at a rate predicted by the equation:

$$R_d = 270t \ . \tag{3-1}$$

With the assumption of a constant heater surface temperature under the evaporating microlayer, an equation was derived for initial microlayer thickness of the following form:

$$\delta_i^2 = \frac{2\alpha \, C_p(T_{hs} - T_s) \, \tau}{h_{fg}} \ . \tag{3-2}$$

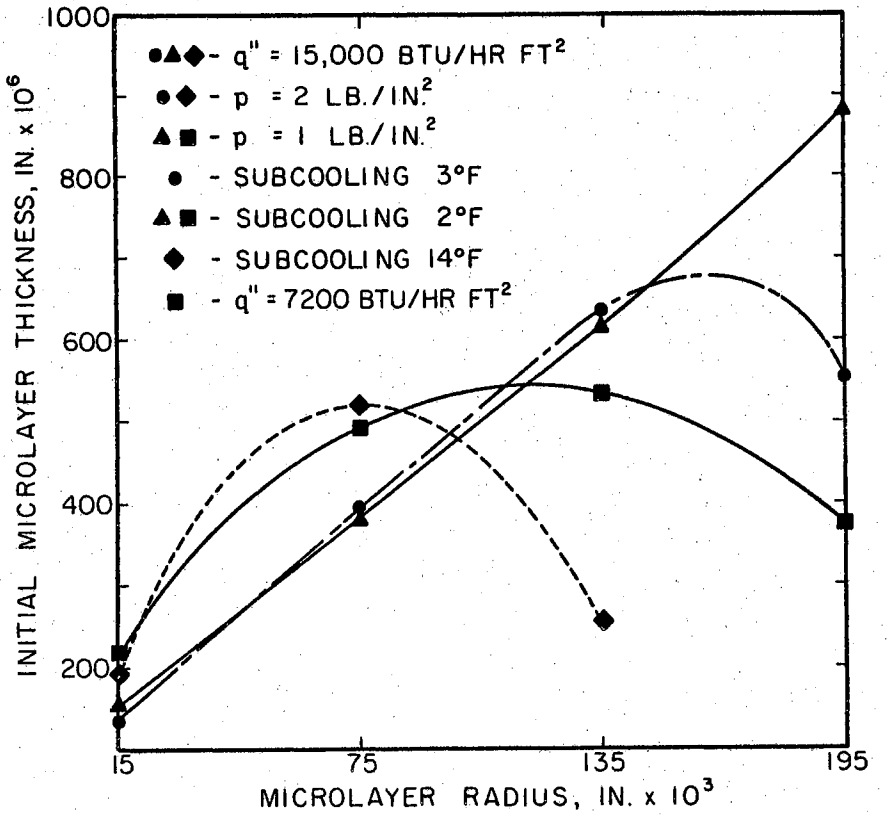

Figure 6. Initial Microlayer Thickness vs Bubble Radius (Ref. 4)

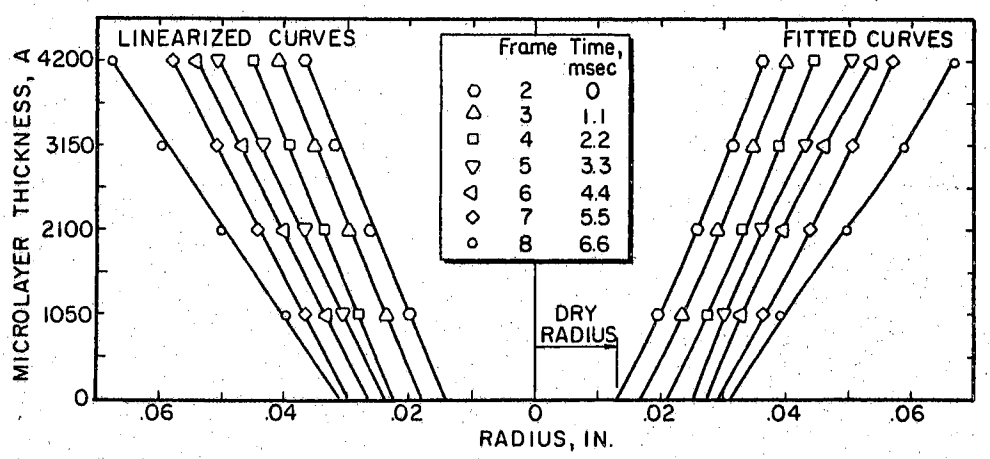

Figure 7. Instantaneous Microlayer Thickness vs Bubble Radius with Time the Parameter (Ref. 24)

The simultaneous solution of equations (3-1) and (3-2) and the substitution of experimental conditions resulted in a variation of δ_i with radius of the form:

$$\delta_i = 1.58(10^{-4}) \sqrt{r} \ . \qquad (3\text{-}3)$$

A plot of this equation is shown in Figure 8.

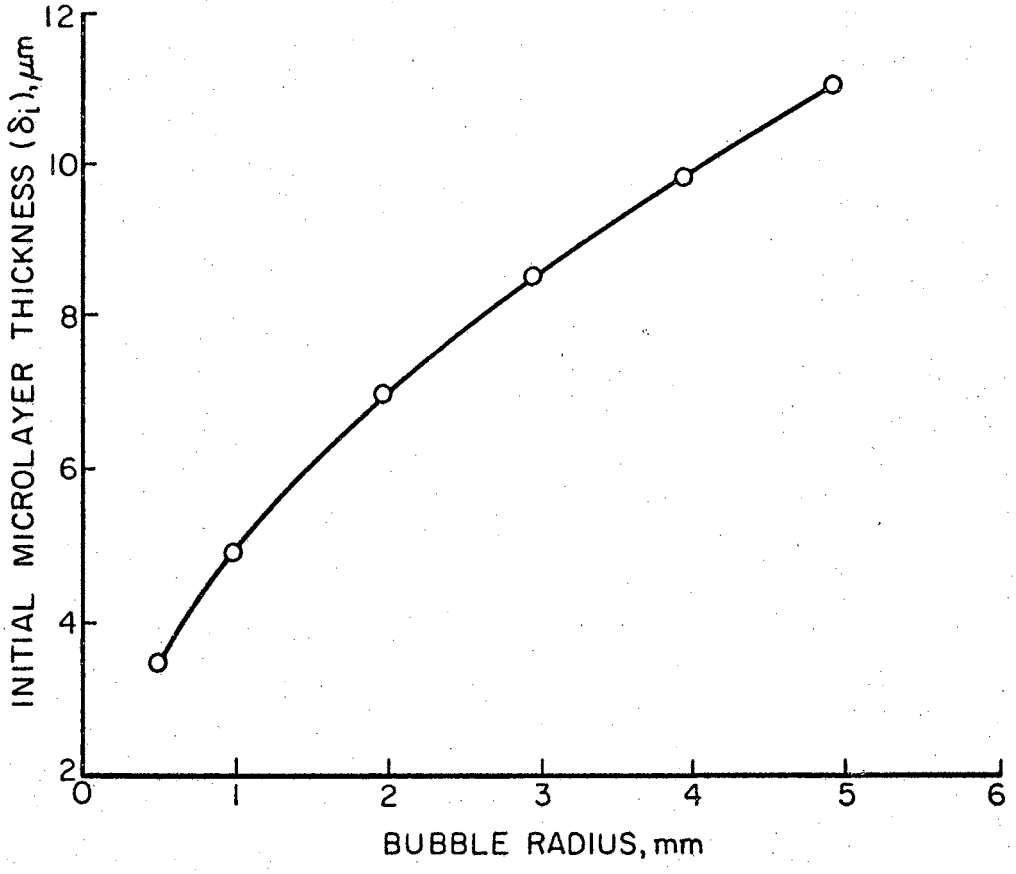

Figure 8. Initial Microlayer Thickness vs Bubble Radius (Ref. 15)

Jawurek [14] measured microlayer profiles which did not continue to decrease in thickness during evaporation at all radii. Instead, a decrease in thickness was observed in a central region which eventually evaporated to dryness while an increase occurred at larger radii indicating an inflow of fluid around the bubble perimeter. This increase in thickness with time is illustrated in Figure 9.

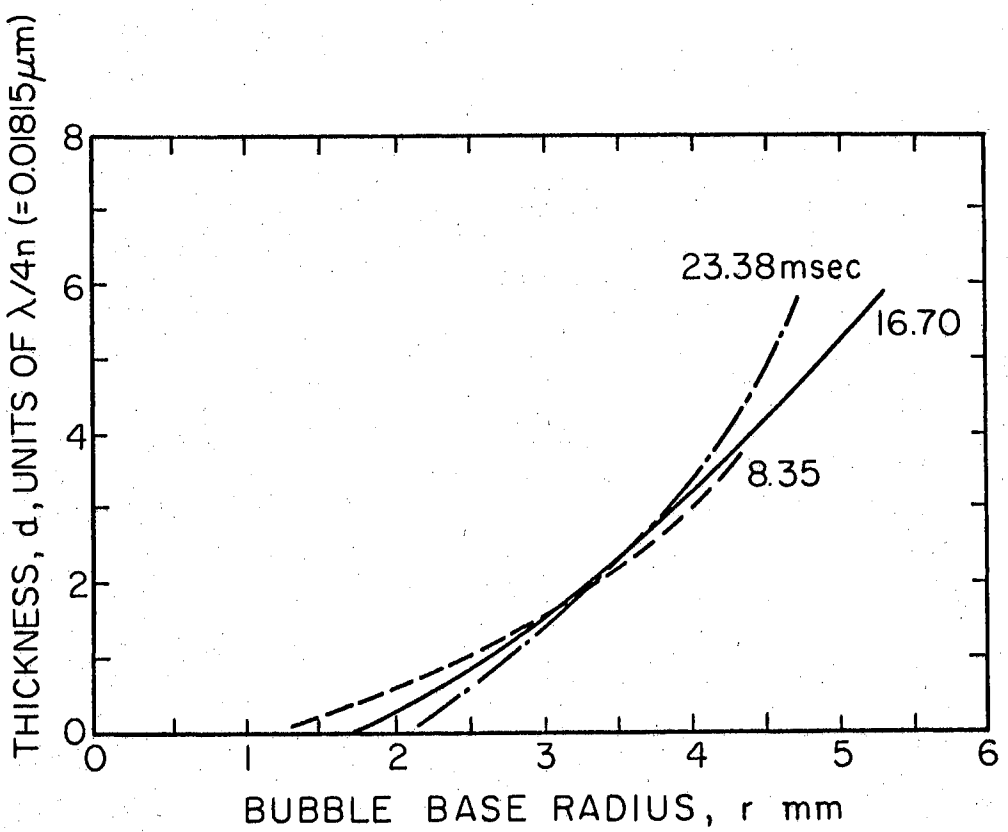

Figure 9. Instantaneous Microlayer Profiles (Ref. 14)

Before microlayer vaporization can be fully understood, data must be obtained on how the microlayer forms as well as on how it evaporates as a function of both radius and time; i.e., both initial and instantaneous information is needed for a single bubble over its entire radius and during its entire lifetime. Except for the very recent work by Jawurek [14], the above investigations fell short of obtaining such extensive data.

Cooper and Lloyd [4] [5] estimated δ_i at four radial positions but no information on δ was reported. The δ_i information illustrated in Figure 6 was not conclusive as to linearity or nonlinearity. Radial information was lacking; bubbles were grown with a maximum radius of 0.7 inches, but data was taken only to a radius of 0.195 inches. Therefore, data was taken over only 34 percent of the maximum radius.

Sharp [24] recorded data on δ but δ_i information was impossible for him to obtain as he had to wait until a bubble grew up and flattened against a plastic window before the microlayer could be photographed. Because of the limitations posed by this technique, photography was possible only in the middle of bubble growth and only in a region of the microlayer where evaporation had begun long before the first frame was exposed. Since the field of view was limited by the flattened area in contact with the plastic window, data could be obtained over only 18 percent of the maximum bubble radius. The effect on the microlayer of having the bubble dynamically constrained could not be determined.

Katto and Yokoya [15] coupled their experimental data on the expanding dry radius phenomena with an analytical approach to arrive at values of δ_i. However, the constant wall temperature assumption

in their analytical approach is certainly open to question as several other investigators ([4],[9],[21]) have shown that the wall temperature does indeed drop dramatically during microlayer vaporization. Here again it was impossible to determine the effect of the dynamic constraint imposed by the interference plates.

Jawurek's [14] experimental work, contrary to the thinking of earlier investigators, indicated perimeter inflow into the microlayer.

Analytical Techniques

The examination of the publications of previous investigators revealed the need for more extensive microlayer-thickness data taken under natural growth conditions. For this investigation the indirect approach was taken of relating microlayer thickness to conduction heat transfer at the heater surface. This approach allowed information on microlayer geometry to be obtained without dynamically constraining the bubble growth. A relationship was derived by the application of a first law energy balance to an evaporating microlayer. If the microlayer, shown in Figure 10, is treated as a closed system while the process is traced on a temperature-entropy diagram, a first law analysis leads to:

$$
\begin{aligned}
du &= \delta q - \delta w \\
&= \delta q - Pdv \qquad\qquad P = \text{Constant} \\
\delta q &= du + Pdv \\
&= dh \\
&= h_3 - h_1 = (h_3 - h_2) + (h_2 - h_1) \\
&= h_{fg} + C_p(T_2 - T_1) \\
&= h_{fg} + C_p(T_s - T_{ia}) \; . \qquad\qquad (3\text{-}4)
\end{aligned}
$$

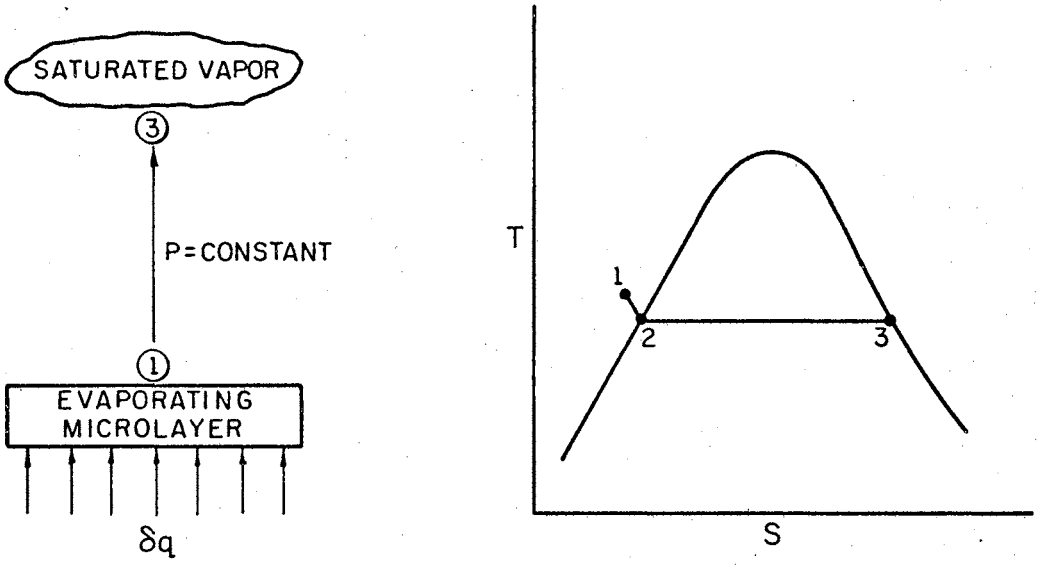

Figure 10. First Law Analysis of Evaporating Microlayer

Therefore, the energy transferred from the underlying solid into the microlayer is equal to the enthalpy of the saturated vapor to which the microlayer vaporizes minus the enthalpy of the microlayer at the instant vaporization began. If a unit area of microlayer is chosen whose initial thickness is δ_i and instantaneous thickness is δ, and if a differential thickness $d\delta$ evaporates in time $d\theta$, Figure 11, then equation (3-4) becomes:

$$q''(\theta) = - \rho_{m\ell} \frac{d\delta}{d\theta} [h_{fg} + C_p(T_s - T_{ia})] \ . \qquad (3\text{-}5)$$

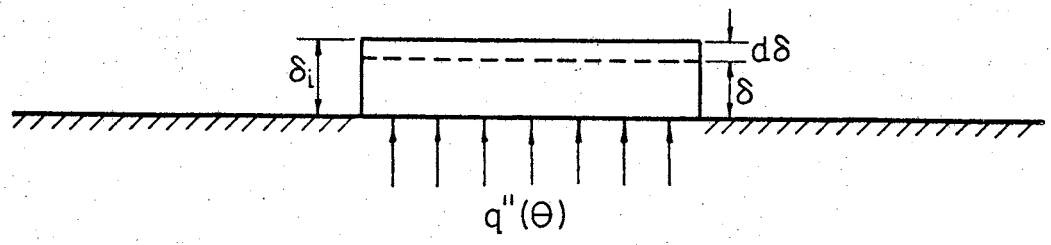

Figure 11. Unit Area of Evaporating Microlayer

T_{ia} in equation (3-5) is a quantity that would be very difficult to measure experimentally, so it is related to more easily measured quantities by the application of the Fourier law at the instant vaporization begins, Figure 12:

$$q_i'' = K_{m\ell} \frac{\Delta T}{\Delta x} = K_{m\ell} \frac{T_{ihs} - T_{ia}}{\delta_i/2} ;$$

$$T_{ia} = T_{ihs} - \frac{q_i'' \delta_i}{2K_{m\ell}} . \qquad (3\text{-}6)$$

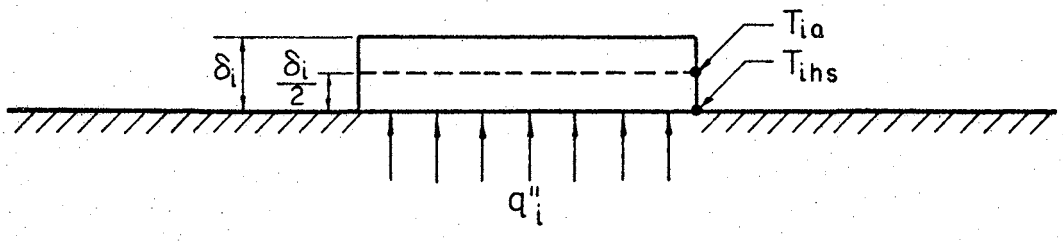

Figure 12. Application of the Fourier Law to a Unit Area of Microlayer to Determine T_{ia}

If equations (3-5) and (3-6) are solved simultaneously, the result is:

$$q''(\theta) = - \rho_{m\ell} \left[h_{fg} + C_p(T_s - T_{ihs}) + \frac{C_p\, q_i''\, \delta_i}{2K_{m\ell}}\right] \frac{d\delta}{d\theta} . \qquad (3\text{-}7)$$

Now the variables can be separated in (3-7) and the left-hand side integrated from zero time to some time θ while the right-hand side is integrated from δ_i to δ:

$$\int_0^\theta q''(\theta)d\theta = - \int_{\delta_i}^{\delta} \rho_{m\ell} \left[h_{fg} + C_p(T_s - T_{ihs}) + C_p \frac{q_i''\, \delta_i}{2K_{m\ell}}\right] d\delta \; ;$$

$$\int_0^\theta q''(\theta)d\theta = (\delta_i - \delta)\, \rho_{m\ell} \left[h_{fg} + C_p(T_s - T_{ihs}) + C_p \frac{q_i''\, \delta_i}{2K_{m\ell}}\right] . \qquad (3\text{-}8)$$

Equation (3-8) relates initial and instantaneous microlayer thicknesses during the evaporation process. If the microlayer evaporates to dryness in some time τ, then as $\theta \to \tau$, $\delta \to 0$, and equation (3-8) reduces to:

$$0 = \frac{\delta_i^{\,2}\, \rho_{m\ell}\, C_p\, q_i''}{2K_{m\ell}} + \delta_i\, \rho_{m\ell} \left[h_{fg} + C_p(T_s - T_{ihs})\right] - \int_0^\tau q''(\theta)d\theta . \qquad (3\text{-}9)$$

Therefore, once evaporation to dryness occurs at any radial position, equation (3-9) can be used to obtain the initial microlayer thickness δ_i. Once δ_i is known for any radial position, equation (3-8) can then be applied to obtain δ at any time from zero to τ during the evaporation to dryness.

Equations (3-8) and (3-9) contain the terms $q''(\theta)$ and q_i'' which must come from a conduction analysis of the underlying solid during

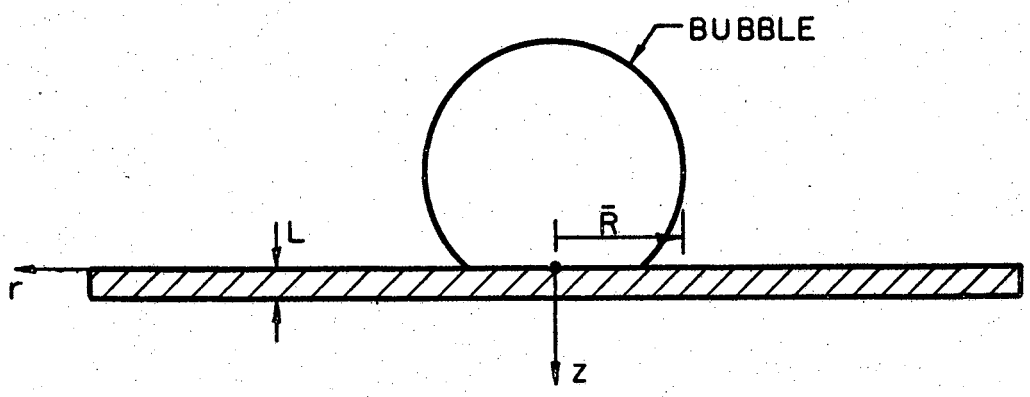

Figure 13. Two-Dimensional Cylindrical Coordinate System

bubble growth. The partial differential equation describing this conduction is:

$$\frac{\partial^2 T}{\partial r^2} + \frac{1}{r}\frac{\partial T}{\partial r} + \frac{\partial^2 T}{\partial z^2} = \frac{1}{\alpha}\frac{\partial T}{\partial \theta} \quad . \tag{3-10}$$

The coordinate system is shown in Figure 13. Equation (3-10) is a two-dimensional, cylindrical coordinate Fourier equation. It is first order in time, and second order in r and z. Therefore, it requires an initial condition, two boundary conditions on r and two boundary conditions on z for its solution. The initial condition is:

$$T(r,z,0) = T(r,z) \quad . \tag{3-11}$$

The two boundary conditions on r are:

$$\frac{\partial T(0,z,\theta)}{\partial r} = 0 \quad ; \tag{3-12}$$

$$T(\bar{R},z,\theta) = \text{Constant} \quad . \tag{3-13}$$

The two boundary conditions on z are:

$$T(r,L,\theta) = \text{Constant} \; ; \tag{3-14}$$

$$T(r,0,\theta) = T(r,\theta) \; . \tag{3-15}$$

The initial condition (3-11) requires that the temperature distribution of the underlying solid be known at the instant of bubble nucleation. Boundary condition (3-12) assumes spherical symmetry of the growing bubble. Condition (3-13) is based on the concept that the thermal disturbance induced by heat extraction from the heater surface by a growing bubble does not propagate in the radial direction beyond $\overline{R}$. $\overline{R}$ has been determined by [9] to correspond approximately to the maximum contact radius. Boundary condition (3-14) indicates that the thermal disturbance from a growing bubble does not propagate very far into the solid in the z direction ([21]) and that the temperature beneath the surface at some distance L is known. Boundary condition (3-15) requires knowledge of the heater surface temperatures beneath a growing bubble. Such information could be obtained from thermocouples, thermistors or any temperature device having a very short time constant. A typical plot of temperature versus time and the corresponding heat flux versus time from such a temperature device as it reacts to bubble growth is divided into four different stages as shown in Figure 14 [4]:

1. As the bubble perimeter passes over the temperature sensor, heat is conducted from the underlying solid into the microlayer. This conduction causes the

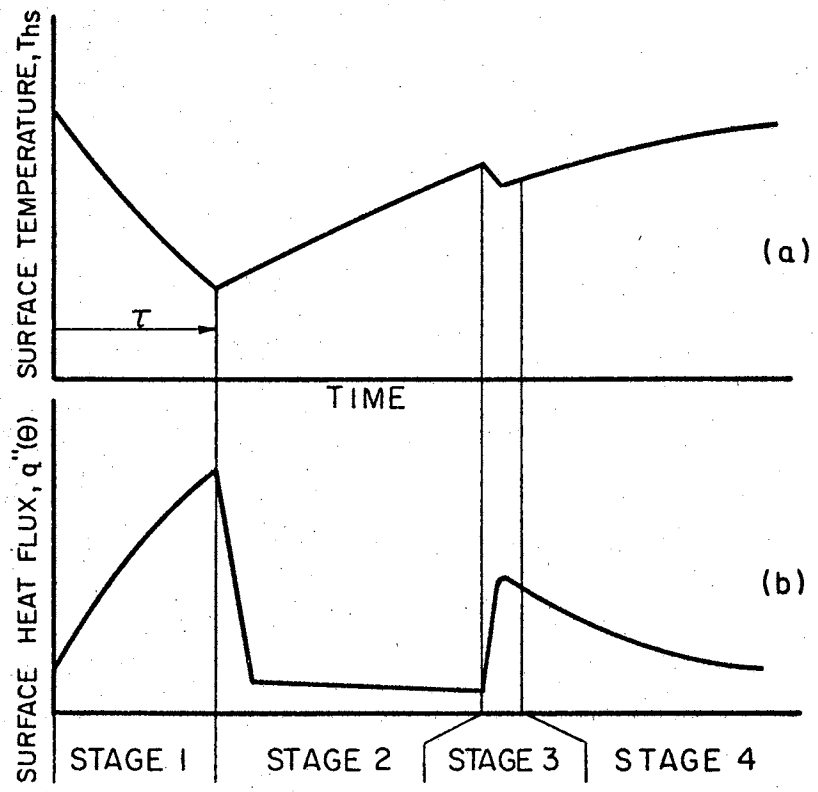

Figure 14. Surface Temperature and Surface Heat Flux vs Time During Bubble Growth at One Temperature Sensor Location (Ref. 4)

microlayer to evaporate at a fast rate with an accompanying fast drop in heater surface temperature.

2. When the microlayer evaporates to dryness, heat is transferred at a reduced rate from heater surface to the vapor, and a surface temperature rise accompanies the thermal recovery in the solid.
3. As the bubble lifts from the surface, cool fluid fills the void and temporarily quenches the solid.
4. A normal thermal layer is reformed.

When initial condition (3-11) and boundary conditions (3-13) through (3-15) are determined experimentally, a computer solution of equation (3-10) can be conducted to determine both the temperature distribution in the solid and the surface heat flux during bubble growth. Then $q''(\theta)$ and T_{ihs} can be substituted into equation (3-9) for the solution of δ_i as a function of radius. With δ_i, $q''(\theta)$ and T_{ihs} known, equation (3-8) can be solved for δ at any time during evaporation. With both δ_i and δ known, microlayer geometry is specified.

Now the question may arise as to the value of the preceding theory if evaporation to dryness does not occur over the entire bubble radius. If such is the case, considerable information about microlayer geometry can still be obtained. For example, consider the hypothetical case of eight temperature sensors in the area of an evaporating microlayer. This process is illustrated in Figure 15 where both δ and δ_i are plotted against sensor number. The segment Md' represents δ_i while d'e' represents extrapolated δ_i. The dashed lines aa', bb', etc. are δ profiles at specific times during bubble growth.

At 1 msec after nucleation, the bubble perimeter has reached sensor 1 and evaporation Maa' has taken place. After 5 msec, the perimeter has reached sensor 3 and evaporation MNbb' has occurred. When 9 msec have lapsed, the bubble perimeter has reached sensor 4, and evaporation MNcc' is complete. However, something new is also evident in that evaporation to dryness has occurred at sensors 1 and 2. As the process continues, evaporation to dryness occurs at six sensors, and the instantaneous profile reaches ee' at which time the bubble lifts from the surface. Now, what information can be determined from the analytical development in the 'wet' region ed'e'?

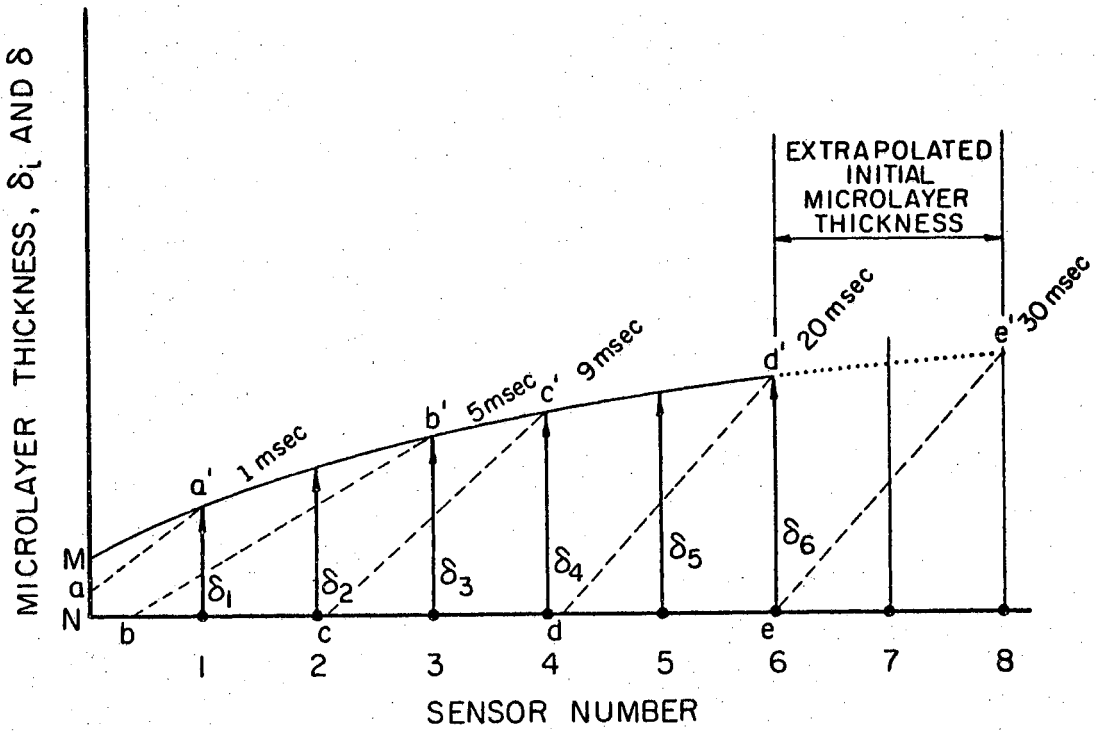

Figure 15. Hypothetical Initial and Instantaneous Microlayer Thickness vs Sensor Number

At the six sensors where evaporation to dryness occurred, equation (3-9) can be solved to obtain δ_1, δ_2, δ_3, etc. Once the δ_i information is available, equation (3-8) can be solved to obtain the δ profile at any time during the evaporation. Now consider the 'wet' region where evaporation to dryness did not occur. Information can be obtained in this region by first performing the extrapolation d'e' in Figure 15. Once the extrapolation from the 'dry' to 'wet' region is completed, δ_i information necessary for the solution of equation (3-8) is available, and δ at any time during evaporation in the 'wet' region can be calculated. Thus, an extrapolation of δ_i from the 'dry' region to

the 'wet' region allows a complete solution for the microlayer geometry during the entire bubble lifetime, over the entire bubble radius.

Experimental Objectives

The preceding development describes a method of determining microlayer geometry by coupling a conduction analysis in the heater solid to a first law analysis of an evaporating microlayer. The entire approach hinges on the experimental determination of initial condition (3-11) and boundary conditions (3-13) through (3-15). Once these conditions are known, equation (3-10) can be solved. With the information from the solution of (3-10), equations (3-9) and (3-8) are then solvable for initial and instantaneous microlayer profiles.

The application of the above procedure to determine initial and instantaneous microlayer thicknesses from experimental temperature measurements was the goal of this investigation. The investigation was performed in two steps:

1. Apparatus was designed and constructed to determine experimentally conditions (3-11), (3-13), (3-14), and (3-15).
2. Equations (3-8), (3-9), and (3-10) were solved to obtain the microlayer profiles.

CHAPTER IV

EXPERIMENTAL APPARATUS

The apparatus designed and constructed to obtain the initial and boundary conditions for the solution of equation (3-8) was simple in purpose but rather complicated in structure. In purpose the apparatus had to:

1. Nucleate a bubble at a prescribed time at a specified location on the heater surface;
2. Record the temperature in the solid at some depth L during bubble growth;
3. Record radial temperatures on the heater surface beneath the expanding bubble during its entire lifetime;
4. Photograph the bubble during its growth,

all with synchronization.

Function and Operation

A schematic of the apparatus, Figure 16, illustrates a boiler in which a bubble is grown while it is photographed and while temperatures are recorded at the heater surface beneath the bubble. A complete list of specifications for all of the experimental apparatus can be found in Appendix A. The temperatures are measured by vacuum-deposited thermistors and recorded by a galvanometer recorder. The Goose Controller is

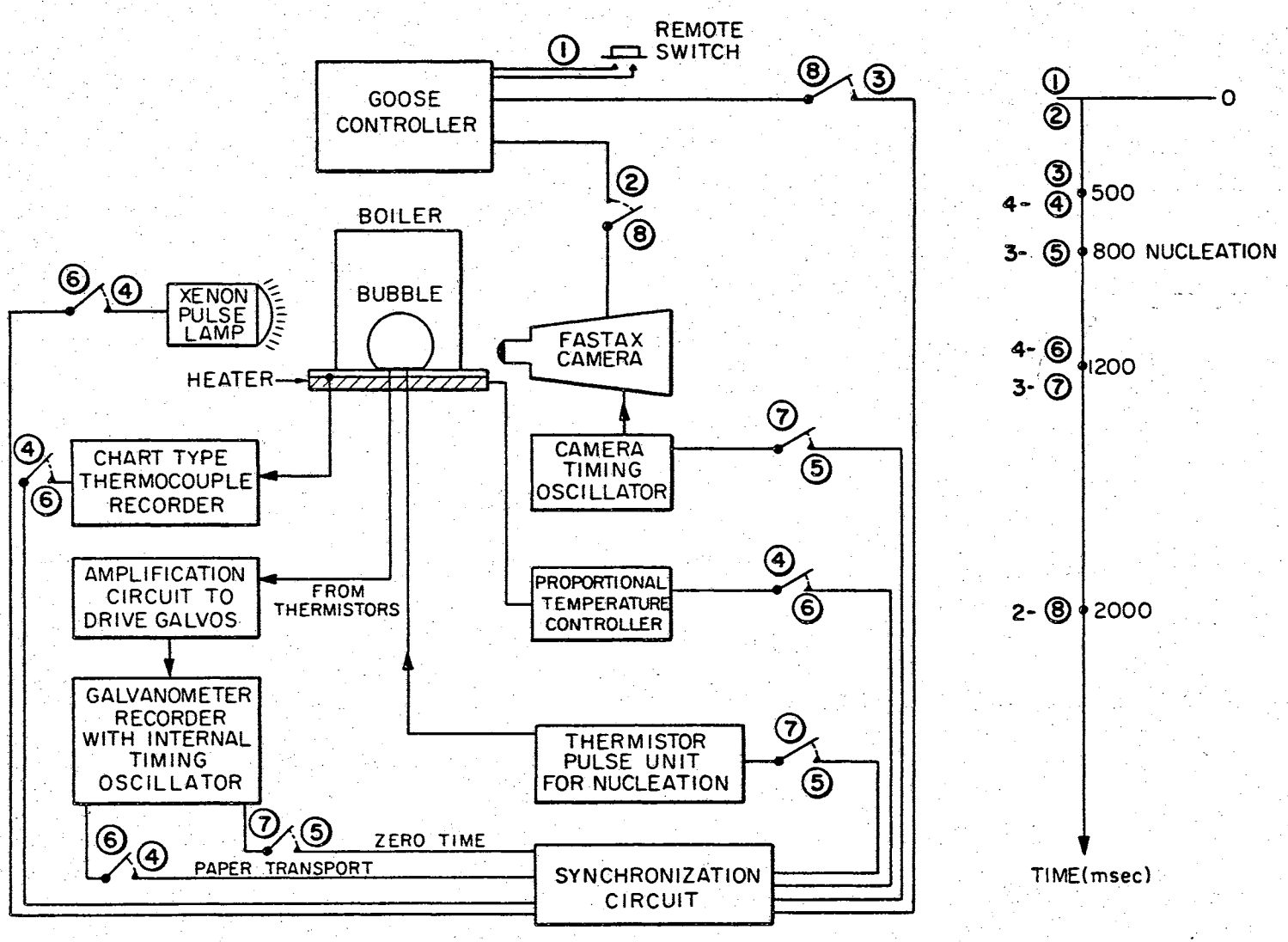

Figure 16. Apparatus Schematic

a variable DC voltage source for controlling camera frame rate. The Xenon pulse lamp illuminates the boiler during photography. The synchronization circuit is the master control for all of the apparatus.

The fictitious switches shown in Figure 16 represent events in time rather than being actual pieces of hardware, i.e., the switch in the upper right, above the camera, illustrates that the camera is armed the second event in time and disarmed the eighth event in time.

A data-taking sequence begins when the 'remote' switch is closed. This closure arms the Goose Controller which begins bringing the camera up to speed. When the camera is up to the desired frame rate, one of the Controller's timers closes a set of external contacts. This closure energizes the synchronization circuit. As the synchronization circuit is energized, it performs four simultaneous operations:

1. Starts the galvanometer recorder's paper drive unit. The paper drive unit requires 250 msec to come up to a uniform transport speed.
2. Stops the paper drive motor on the thermocouple recorder. This temporary halt of the paper produces a flat spot on the temperature-time trace; the flat spot synchronizes the temperature recorded to the time of data taking.
3. Turns off the proportional temperature controller. This temporary interruption of the controller eliminates the electrical noise from the controller's gated SCR during data taking.
4. Turns on the Xenon pulse lamp circuit.

Two hundred fifty milliseconds after the above four events, the synchronization circuit performs three more simultaneous operations:

1. Arms the thermistor pulse unit; the pulse unit immediately sends a single rectangular voltage pulse to an outer thermistor whose self heat from the pulse forms a small vapor nucleus which acts as the nucleation site for bubble growth.
2. Arms the camera timing oscillator; the oscillator immediately begins sending 1000 rectangular pulses per second to the camera's timing neon.
3. Applies a voltage pulse to one recorder galvanometer; this pulse synchronizes bubble nucleation with the recorder data from the thermistors.

The apparatus is now ready to record data as the growing bubble encounters the radially positioned thermistors. As the thermistors experience the temperature fluctuations, their signals are amplified and fed to the galvanometer recorder. The important data is collected in approximately 100 msec, but the apparatus is allowed to run for an additional 300 msec to check for secondary nucleations or other disturbances on the heat transfer surface. A secondary nucleation is a nucleation that occurs at a natural site after the voltage pulse has been applied to the edge thermistor.

At the end of data taking the synchronization circuit performs seven more operations:

1. Stops the paper transport of the galvanometer recorder.
2. Starts the paper transport of the thermocouple recorder.

3. Turns on the proportional temperature controller.
4. Turns off the Xenon pulse lamp circuit.
5. Disarms the thermistor pulse unit.
6. Disarms the camera timing oscillator.
7. Drops the voltage pulse to the recorder galvanometer used to synchronize nucleation with the other galvanometer traces.

Eight hundred milliseconds later, the Goose Controller times out and disarms the camera and synchronization circuit. A total data-taking sequence takes approximately two seconds. A time flow for the various data-taking events is illustrated along the right side of Figure 16.

Much of the apparatus in Figure 16 was constructed specifically for this boiling investigation. The more important pieces of this hardware will now be described in detail.

Synchronization Circuit

The synchronization circuit, Figure 17, is the master control for all of the apparatus during data taking. As the contacts of K_5 close at the Goose Controller, V_B is pulled to ground. This reverse biases Q_1 which stops conducting and de-energizes K_1. However, as soon as V_B is pulled to ground, C_1 begins to charge. Capacitor C_1 soon reaches the necessary voltage to again forward bias Q_1 which then re-energizes K_1. During the short time that K_1 is de-energized, K_1 connects V_1 to the coil of K_2, and K_2 closes and latches. Therefore, the purpose of the portion of the circuit containing K_5 and K_3 is to supply a one-shot pulse of the magnitude V_1 to arm relay K_2.

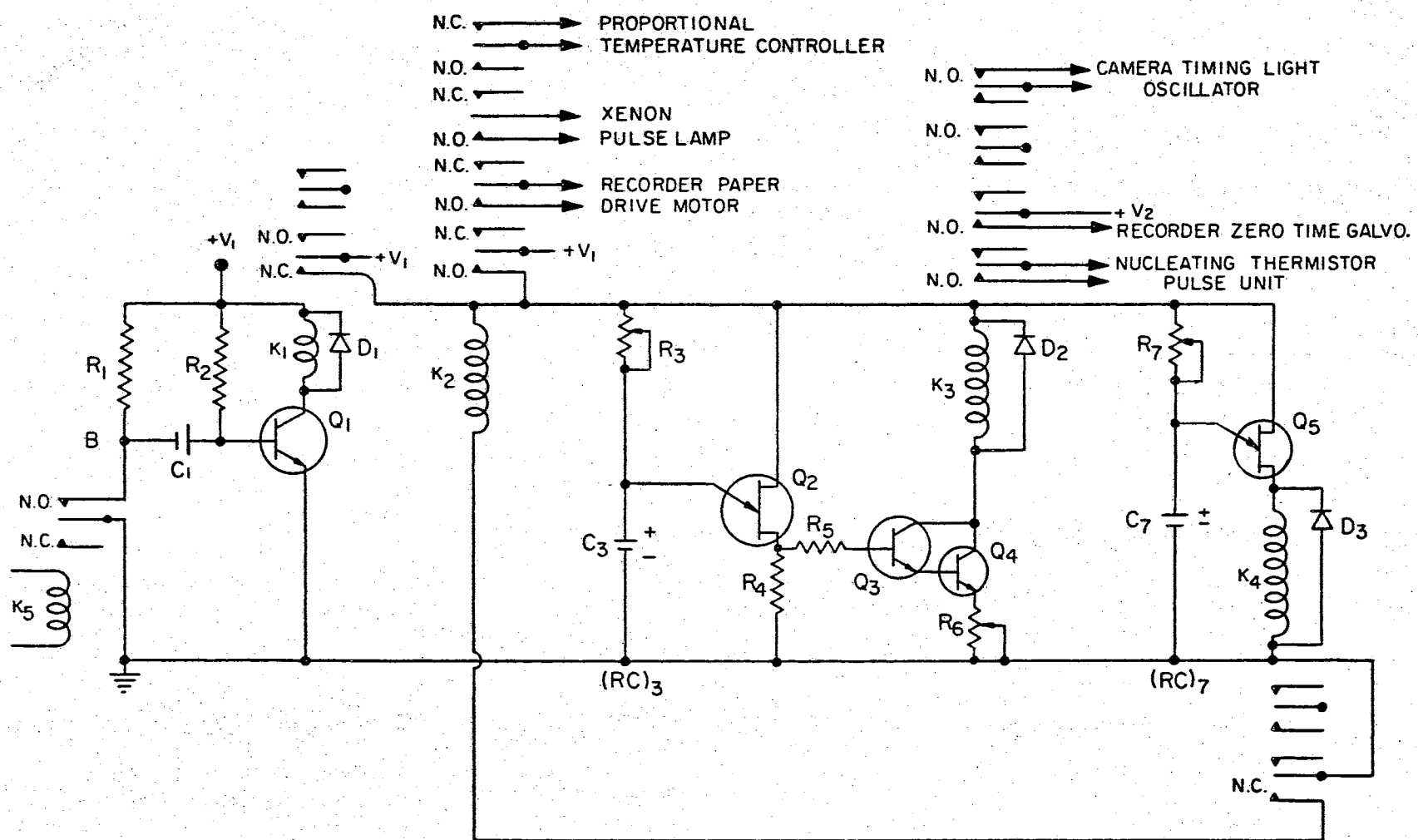

Figure 17. Synchronization Circuit

When K_2 operates, it turns on the recorder paper drive motor and the Xenon pulse lamp and turns off the proportional temperature controller and the thermocouple recorder paper drive. At the same time, K_2 latches and applies a $+V_1$ to all of the circuit to its right. This starts the charging of the two RC networks, $(RC)_3$ and $(RC)_7$. After 250 msec, $(RC)_3$ has reached the necessary voltage to fire Q_2. The firing of the UJT puts the Darlington pair, Q_3 and Q_4, in forward bias thus energizing the coil of K_3. When the contacts of K_3 close, the camera timing oscillator and the thermistor pulse unit are each armed and a $+V_2$ pulse is sent to one of the recorder galvanometers. This pulse synchronizes bubble nucleation with the temperature traces on the recorder. Data taking begins with the closing of K_3. Four hundred milliseconds later, at the end of data taking, $(RC)_7$ has charged to the necessary voltage to fire Q_5 which energizes the coil of K_4. When K_4 operates, K_2 is de-energized. As the contacts of K_2 open, the coil of K_3 is de-energized thus disarming the three circuits fed from the contacts of K_3.

Amplification Circuit

Amplification of each thermistor signal was necessary to convert a change in resistance to a change in current for driving the optical galvanometers in the recorder. The circuit used to amplify each thermistor signal is shown in Figure 18. R_8 limits the self heating of the thermistor by keeping the current level below 10 μA. R_9 and R_{10} provide the proper bias for adjusting the steady state current level to each galvanometer. Since the current requirement of each galvanometer was more than the amplifier could supply, an emitter

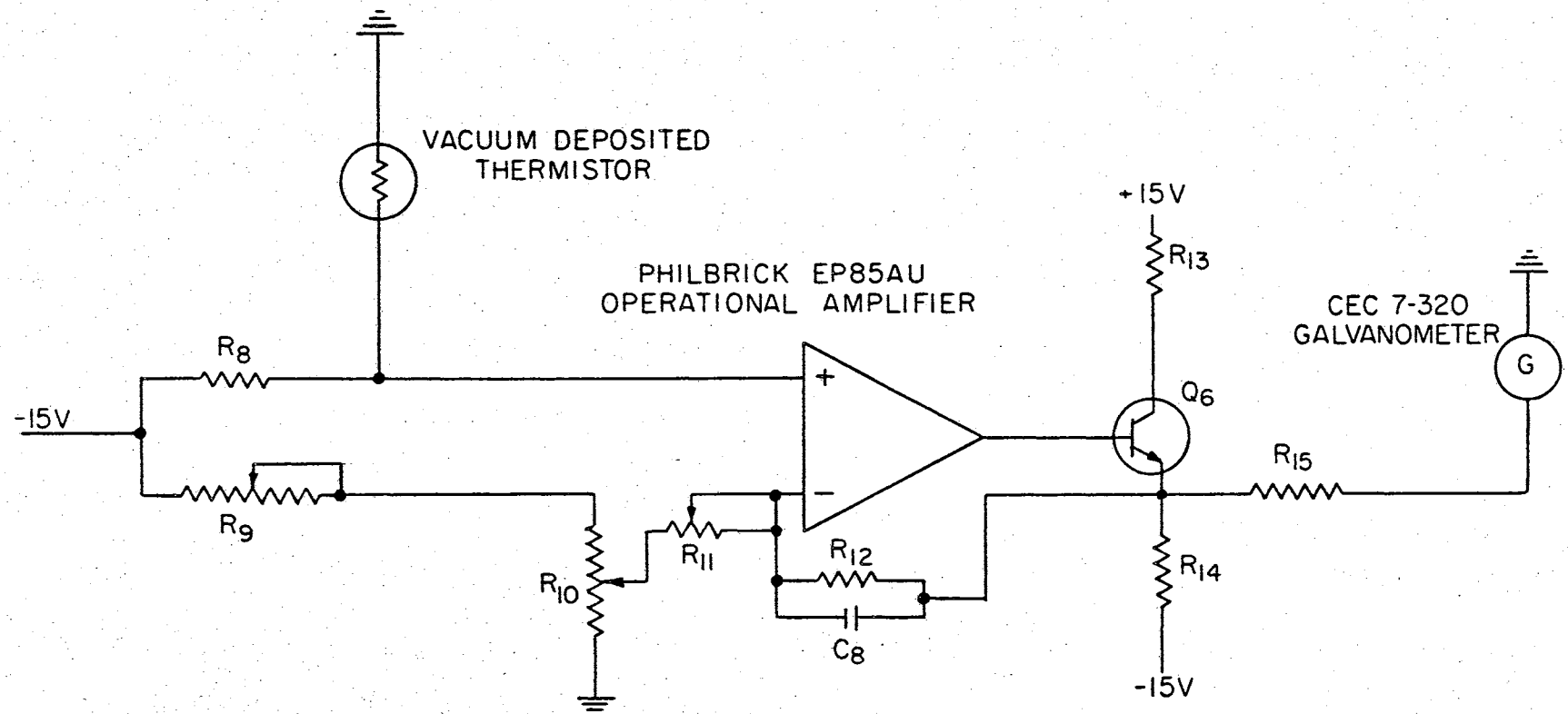

Figure 18. Amplification Circuit

follower, Q_6, was used for current amplification. R_{15} provided the proper galvanometer damping.

During data taking, a plus and minus swing was used to take full advantage of the central linear range of the galvanometers. The amplifier gains were adjusted by changing R_{11} until each galvanometer experienced a suitable swing during bubble growth.

Boiler Assembly

The boiler assembly is illustrated in Figure 19. The boiler is a pyrex cell with a pyrex plate bottom on which were vacuum deposited fifteen thermistors and their leads. A condenser and precision thermometer were attached to the top of the cell. The thermometer measured bulk temperature at nucleation and during thermistor calibration. A cylindrical baffle prevented the condenser from slugging during bubble growth; the baffle was also used to agitate the bulk fluid during thermistor calibration. An aspirator was used to pull a vacuum which was read on a mercury manometer. An air-bleed valve between the manometer and condenser was used to set the boiler vacuum at a specific level. The pyrex bottom of the boiler was heated by a muffle furnace heater through an intermediate, unitemperature aluminum plate. Wood's Metal in the cavity between the aluminum and pyrex assured good thermal contact between the boiler bottom and the aluminum plate. A thermocouple monitored the temperature of the aluminum plate and Wood's Metal. Power was supplied to the muffle furnace heater from a proportional temperature controller.

The thermistor and lead fabrication are described in Appendix B.

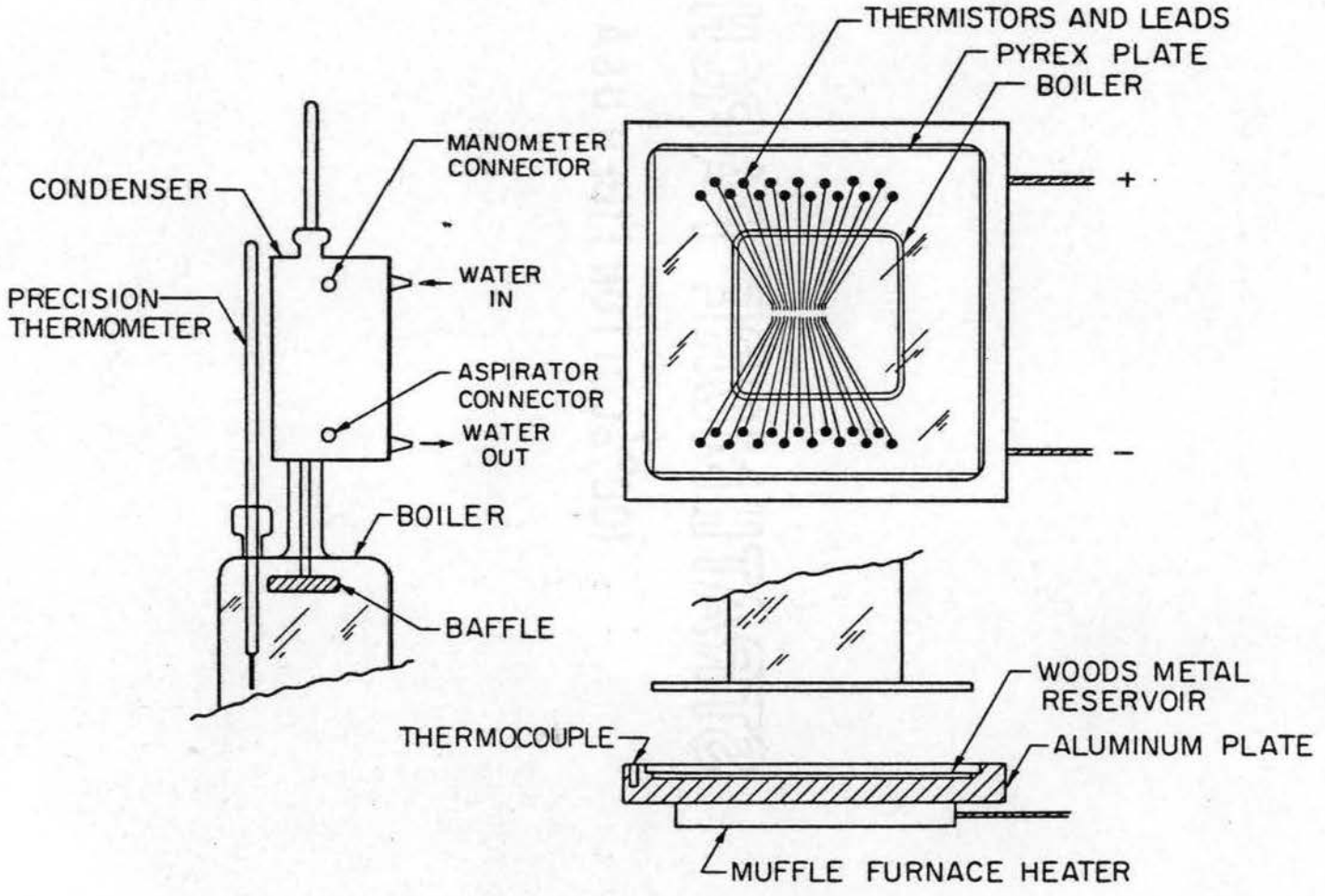

Figure 19. Boiler Assembly

CHAPTER V

ACQUISITION AND PROCESSING OF DATA

A data run for this investigation was a lengthy, tedious process, so only a few of the more than fifty steps will be mentioned. They were:

1. Read barometer.
2. Fill ice bath for cold junction.
3. Clean outside of boiler and coat bottom with high K silicone grease to improve thermal contact with the Wood's Metal.
4. Skim the molten Wood's Metal to remove oxide.
5. Fill boiler with fresh, reagent grade benzene; reflux benzene at reduced pressure to remove dissolved gas and to eliminate natural nucleation sites.
6. Cool bulk fluid and adjust air-bleed valve to set desired boiler pressure.
7. Check all hardware to insure proper operation and synchronization.
8. Load and focus camera; at this stage the camera and Xenon were placed in the manual mode rather than in the automatic mode of operation.

After these steps were completed, several trial bubbles were nucleated with all of the apparatus operating, but with the camera and Xenon lamp still in the manual mode. Each trial bubble was grown by lowering the boiler assembly into the Wood's Metal and observing the bulk temperature and galvanometer beams. When the bulk temperature was increasing and the galvanometer beams were relatively stable, the remote button of Figure 15 was pressed to start the data sequence. At the same time, the bulk temperature was recorded. After the data sequence, the boiler assembly was raised from the Wood's Metal and placed on a Transite stand to cool. The recorder traces were then examined for:

1. Number of thermistors that experienced the temperature disturbance from the bubble.
2. Signs of secondary nucleation.
3. Turbulent or 'clean' lift-off; clean lift-off occurs when a bubble rises from the heat transfer surface as a single vapor globule.

When the recorder data from two consecutive runs was of the desired shape, the camera and Xenon were switched from the manual to the automatic mode. A run was then made with the recorder and the camera in the automatic mode. After this run, the vacuum was dropped, and the boiler was left in the Wood's Metal cavity. When the bulk temperature of the benzene was approximately 80°C, the boiler assembly was again placed on the Transite stand to begin cool-down in preparation for the calibration of the thermistors.

As the bulk liquid slowly cooled, the convection currents began to subside at the bottom of the boiler. When the convection currents

had totally disappeared, the bulk fluid was agitated by vertical reciprocation of the baffle (see Figure 19). When the galvanometer light beams returned to the margin of the recorder paper, a remote button was pressed which caused the recorder to transport paper. The calibration was continued by pressing the remote button at each 2°C drop in bulk temperature as the benzene cooled. Each transport of paper generated ten parallel galvanometer traces; the level of each galvanometer trace corresponded to the temperature read on the precision thermometer. A plot of this galvanometer level as a function of the thermometer reading for each galvanometer was used to obtain temperature as a function of time from the galvanometer traces. Figure 20 is a photograph of a typical set of recorder traces. The majority of traces show one major and one minor temperature excursion during bubble growth. The number on each trace corresponds to the position of the thermistor that generated the trace, i.e., traces 1, 2 and 3 were taken from thermistors located 0.060 in., 0.120 in. and 0.180 in. respectively from the nucleation site. The unnumbered trace at the bottom of Figure 20 was made by the zero-time galvanometer.

Galvanometer levels were taken from the recorder traces at intervals of one millisecond from the time of nucleation until the bubble lifted from the surface. These galvanometer levels were converted to temperatures with the calibration curves. These temperature-time values were then plotted on an IBM 1620 Computer interfaced to a CalComp 565 Plotter; the plot is shown in Figure 21.

Trace numbers 1, 2, 3, 5, 6, 8, 9, 11, 12, and 13 represent actual data. Since boundary condition (3-15) required experimental temperature information over the entire bubble radius, one extrapolation and

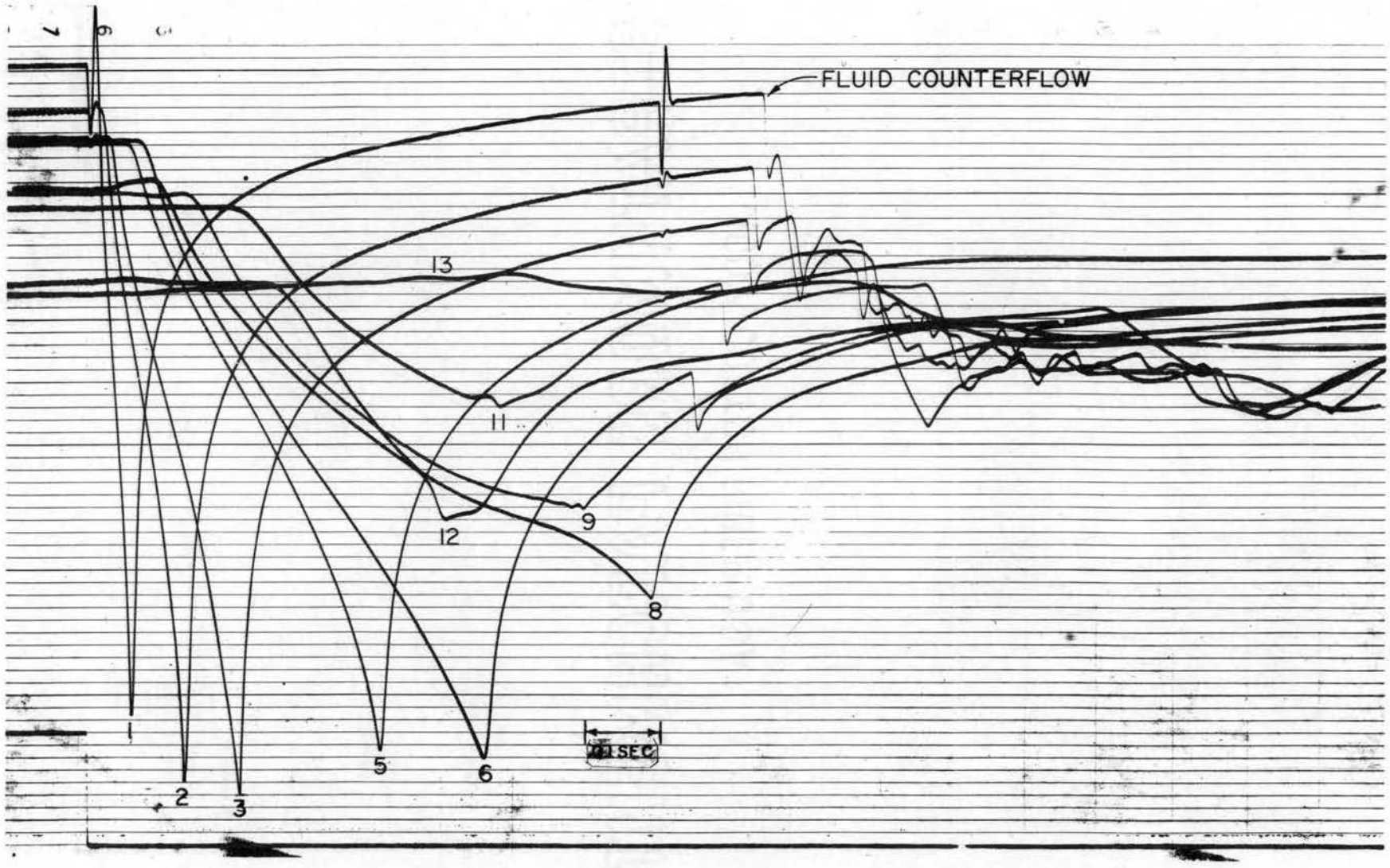

Figure 20. Photograph of Galvanometer Traces

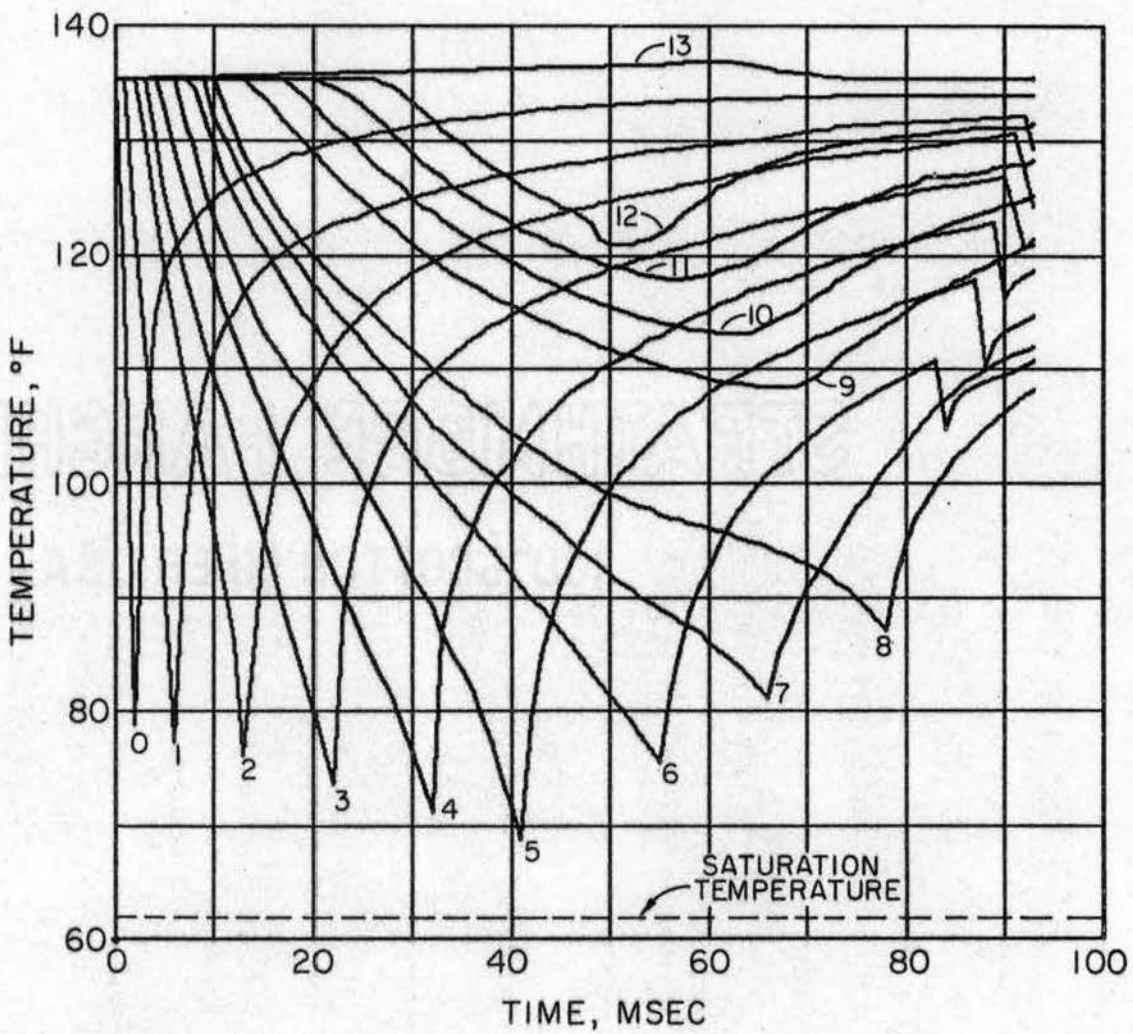

Figure 21. Temperature vs Time for Each Thermistor

three interpolations of the raw data were necessary. Trace 0 was extrapolated from traces 1, 2 and 3. Traces 4, 7 and 10 were interpolated from each pair of surrounding traces (3,5), (6,8) and (9,11) respectively. The extrapolation was necessary because the 0 thermistor could not be used to nucleate a bubble and to measure temperature at the same time. The interpolations were necessary because only ten galvanometers were available to record the signals from fourteen thermistors.

The approach used to solve the conduction heat transfer in the pyrex was to subdivide the glass solid into a system of nodes. The thermal conductance and capacitance of each node were lumped. Then the thermal-electrical analogy was used to transform the problem of heat

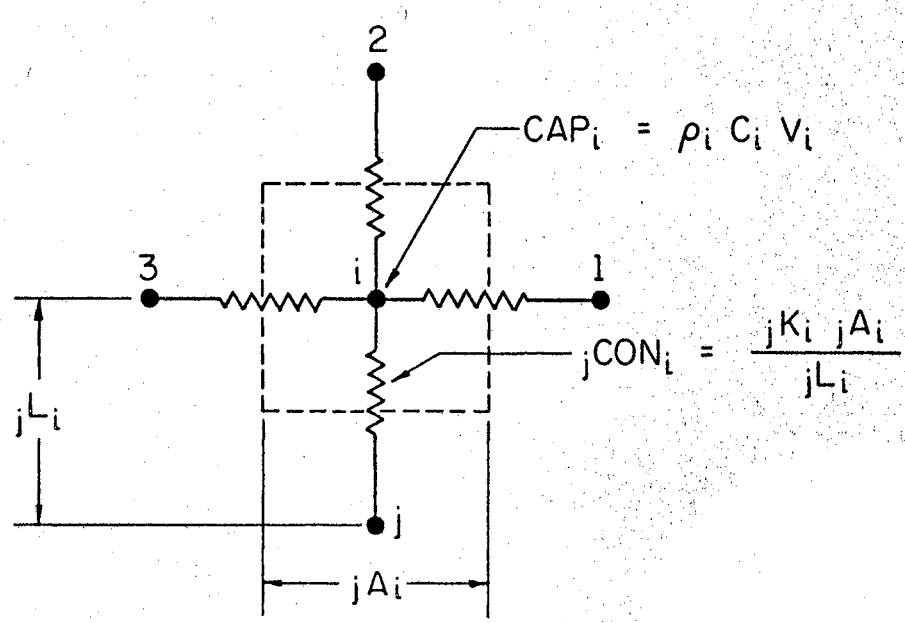

Figure 22. Lumped Parameter Node Model

flow with thermal conductance and capacitance to one of current flow with electrical resistance and capacitance. Each node i with its surrounding nodes j was modeled as illustrated in Figure 22.

A first law analysis of equating the net heat flow to each central node (i) from the surrounding nodes (j) to the gain in internal energy of the central node (i) yields:

$$CAP_i \frac{\Delta T_i}{\Delta\theta} = \sum_j {}_jCON_i \, (T_j - T_i) \, . \qquad (5\text{-}1)$$

If the temperature difference on the left side of (5-1) takes place in a time period from the present (m) to one time step in the future ($m+\Delta\theta$), while the temperatures on the right side are based on future time, equation (5-1) becomes:

$$\frac{CAP_i}{\Delta\theta} (T_{i,m+\Delta\theta} - T_{i,m}) = \sum_j {}_jCON_i \, (T_{j,m+\Delta\theta} - T_{i,m+\Delta\theta}) \, . \qquad (5\text{-}2)$$

If (5-2) is rearranged and solved for $T_{i,m+\Delta\theta}$, the result is:

$$T_{i,m+\Delta\theta} = \frac{\Delta\theta \sum_j {}_jCON_i \, (T_{i,m+\Delta\theta})}{CAP_i + \Delta\theta \sum_j {}_jCON_i} + \frac{CAP_i}{CAP_i + \Delta\theta \sum_j {}_jCON_i} T_{i,m} \, . \qquad (5\text{-}3)$$

Equation (5-3) when written at each node generates a system of simultaneous algebraic equations involving present and future temperatures.

It was necessary to formulate the lumped parameter solution to fit the initial and boundary conditions described by equations (3-11) through (3-15).

At time zero the initial temperature distribution in the solid, equation (3-11), was established by performing a linear interpolation in the z direction between the thermistor temperatures and the thermocouple temperature. This interpolation to establish the distribution

was made possible by assuming that at time zero the heat flow was one dimensional in the z direction. The assumption hinged on two considerations:

1. There was no radial temperature drop at time zero as the glass was surrounded on five sides by a unitemperature Wood's Metal bath.
2. The path for radial heat flow was very long compared to the path for z heat flow.

Boundary conditions (3-12) and (3-13) were treated in the lumped solution by attaching only one radial conductor to the nodes at r = 0 and r = $\overline{R}$. With conductors to carry energy in only one radial direction, this automatically made the gradient zero at r = 0 and r = $\overline{R}$.

Information for boundary condition (3-14) was obtained from the thermocouple embedded in the Wood's Metal bath. The unitemperature liquid metal bath assured that the temperature read by the thermocouple was also the temperature of all of the nodes at z = L.

The information described by equation (3-15) was supplied to the lumped parameter solution from the data used to plot Figure 21.

A FORTRAN IV program was specifically written to solve the conduction problem on an IBM 360/50 Computer. See Appendix C for a program listing. Successive point, Gauss-Seidel iteration was used to solve the system of equations generated by applying equation (5-3) at each node. A linear interpolation was written to obtain the temperatures at each time step at nodes located between thermistors.

When the temperature solution had iterated to tolerance, the heat fluxes at the surface nodes were calculated by applying:

$$q''_{1,j} = {}_1CON_2 \, (T_{1,j} - T_{2,j}) \, . \qquad (5\text{-}4)$$

Figure 23 shows CalComp plots of the surface heat flux at each thermistor as a function of time. The expression

$$\int q''(\theta) d\theta \qquad (5\text{-}5$$

representing an area under each curve in Figure 23 was evaluated for various elapsed times at each thermistor node from the beginning of the major temperature drop until evaporation to dryness. Subroutine QTFE from the IBM/360 Scientific Subroutine Package was used to evaluate the integrals.

After the evaluation of (5-4) and (5-5), equations (3-8) and (3-9) were solved for δ_i and δ, the initial and instantaneous microlayer thicknesses. The computer program used for the solution of (3-8) and (3-9) is listed in Appendix C. Figure 24 illustrates the microlayer thicknesses plotted against thermistor location with time the parameter.

The dry radius information taken from Figure 24 was replotted in Figure 25. Bubble radius, contact radius and thermistor temperatures were also plotted in Figure 25 to synchronize the important phases of the bubble growth. Measurements for the bubble radius and contact radius were taken from the high-speed motion picture film with a Vanguard Motion Analyzer. The frame rate for the photography was 2800 frames per second.

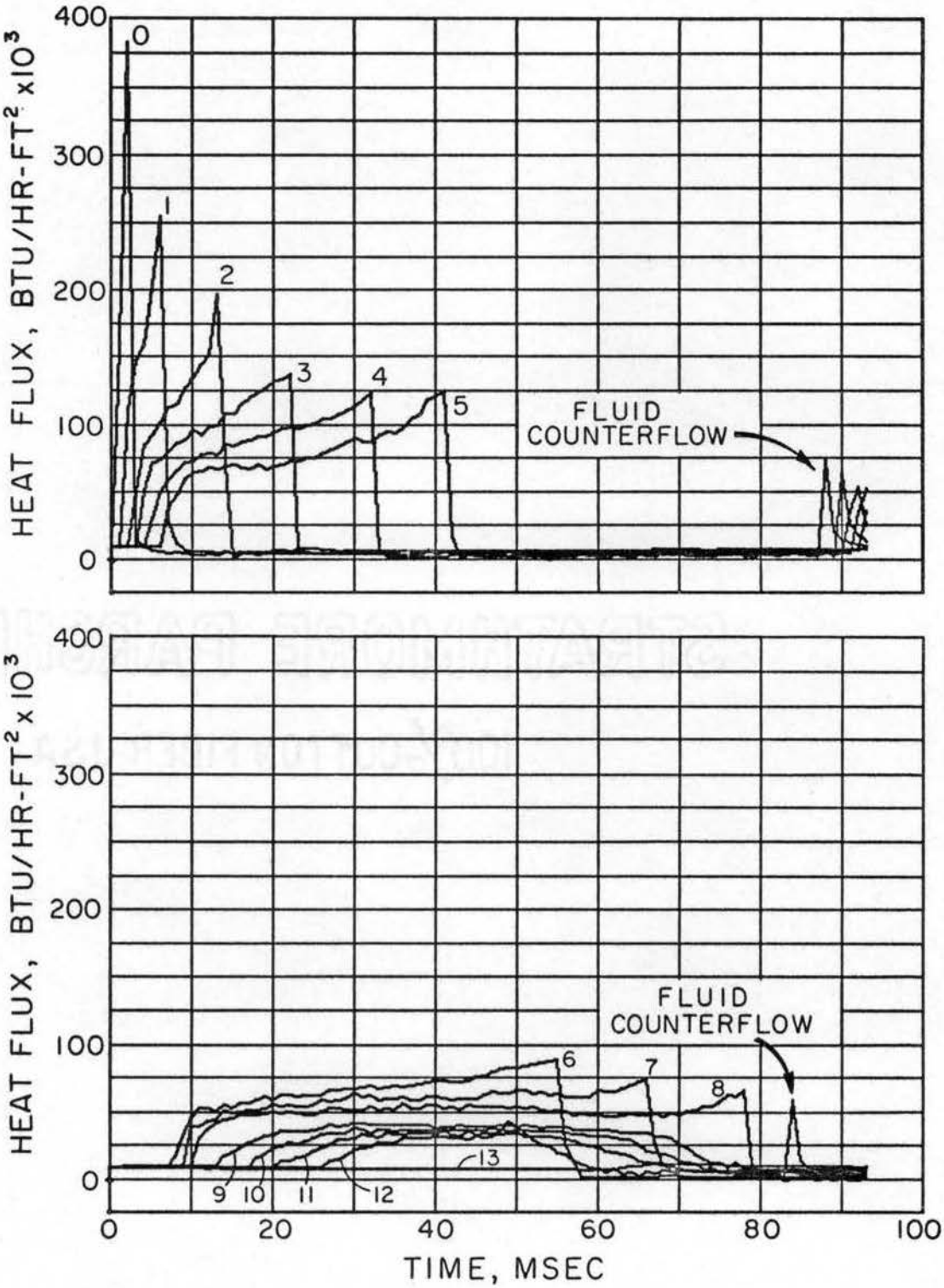

Figure 23. Heat Flux vs Time for Each Thermistor

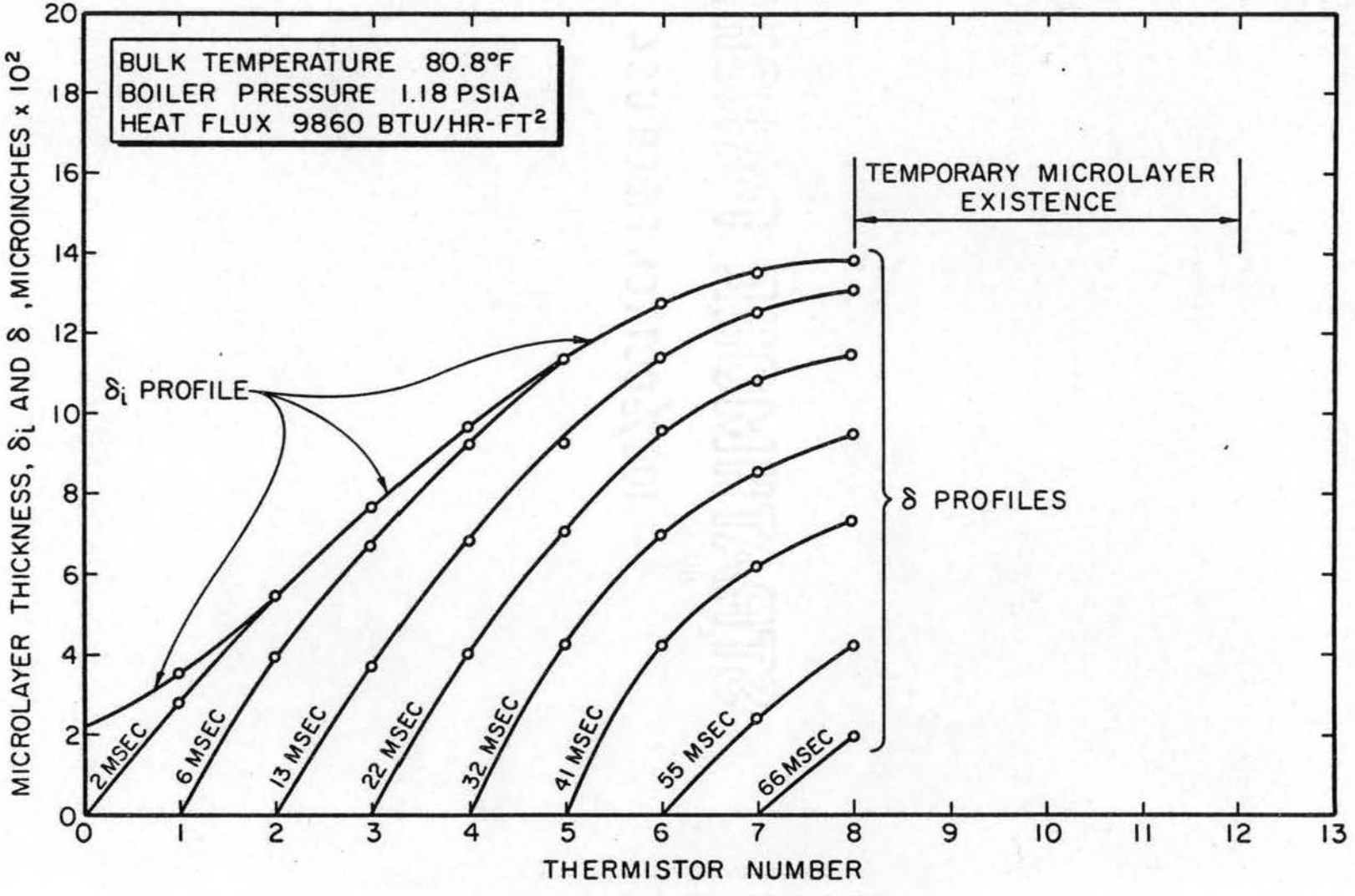

Figure 24. Initial and Instantaneous Thicknesses vs Thermistor Location

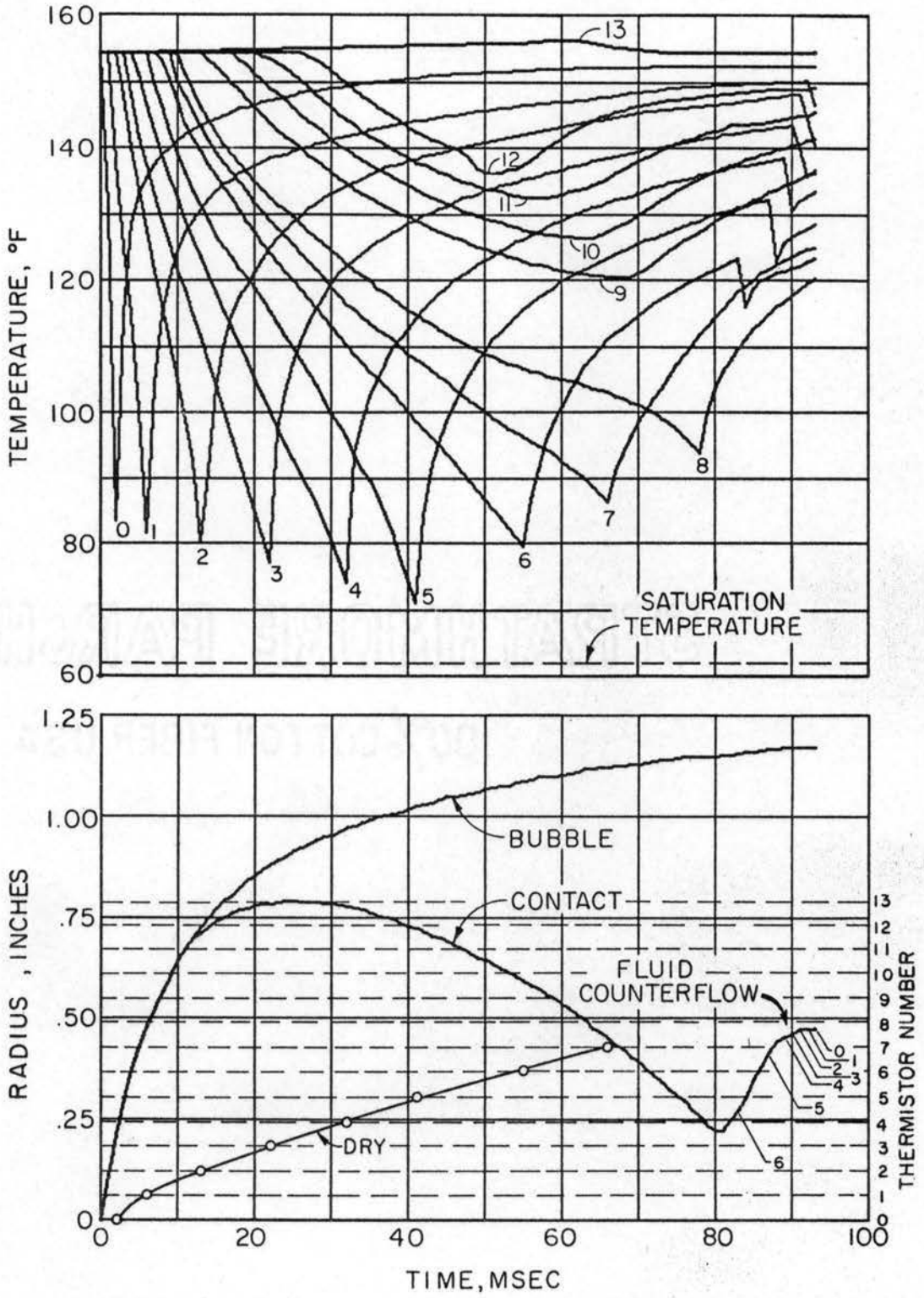

Figure 25. Thermistor Temperature vs Time and Various Bubble Radii vs Time

CHAPTER VI

SUMMARY AND CONCLUSIONS

When the information in Chapter V is compared to the findings of previous microlayer investigators, interesting areas of agreement and disagreement come to light. One of these areas concerns the time of each major temperature drop during bubble growth.

Hendricks and Sharp [9] found that a rapid temperature drop occurred as the perimeter of the bubble base passed over their thermocouple junction. Their photographs indicated that they associated bubble base perimeter with contact diameter.

Cooper and Lloyd [4] in their discussion on the beginning of the major temperature excursions stated:

> Comparison with the high speed film shows that the start at each thermometer occurs approximately when the normal projection of the bubble onto the wall passes the thermometer, as reported by Hendricks and Sharp (6).

Evidentally, Cooper and Lloyd interpreted the "perimeter of the bubble base" from the work of Hendricks and Sharp [9] to mean projected bubble perimeter instead of contact perimeter. However, the sketches of bubble profiles in Run 4 [4] even contradicted this interpretation. In Run 4, the normal projection passed over four thermometers, but temperature drops were recorded at only three.

Figure 25 illustrates that, at the inner radii, the temperature drop began slightly after the contact and coincident bubble radii passed over the thermistor. At approximately 12 msec, the contact

radius separated from the bubble radius as the bubble departed from a hemispherical shape. From the time of radii separation until lift-off, the propagation of the temperature disturbance was more closely related to the motion of the contact radius than to the motion of the projected bubble radius. This is best illustrated by noting that the maximum bubble radius was 1.175 inches while the temperature disturbance did not quite each thermistor 13, or 0.78 inches. The position of thermistor 13 approximately corresponded to the location of the maximum contact radius.

Another area of interest concerning the information in Chapter V and previous work concerns Stage 3 of Figure 14. This stage, showing a minor temperature drop during the recovery from the major temperature drop, has been reported only by Cooper and Lloyd [4]. They associated the minor drops at their four thermometers with bubble lift-off. At lift-off, cool bulk fluid was thought to rush in under the departing bubble to cause a quenching of the heater surface from the outer to inner thermometers.

The minor temperature excursions recorded in this investigation are illustrated in Figures 20, 21 and 25. When the motion picture film was slowly projected through the time of the minor drops, the bubble was observed to grow into a mushroom shape having a stem capped with an umbrella-like top. A short time after the contact diameter passed through the minimum shown in Figure 25, a turbulent stream of fluid droplets imploded from the top of the stem into the bubble interior, Figure 26 (a). The turbulent stream soon filled the bubble interior with a spray of droplets, Figure 26 (b). The minor temperature excursions occurred at the time of the implosion of the turbulent stream.

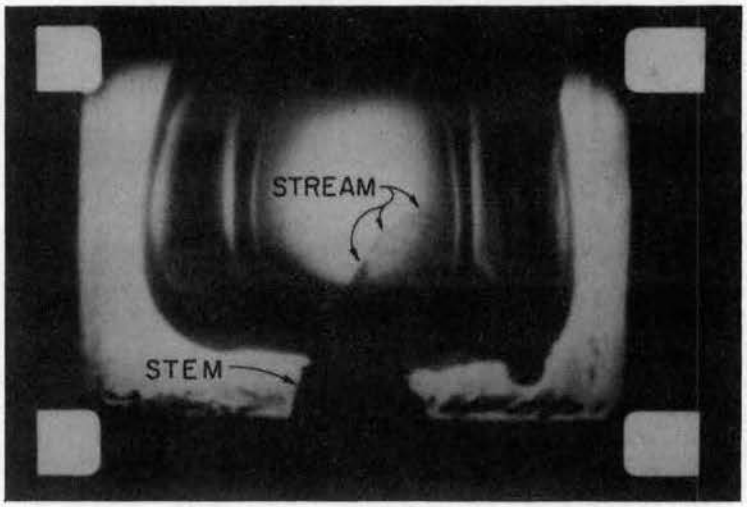

(a)

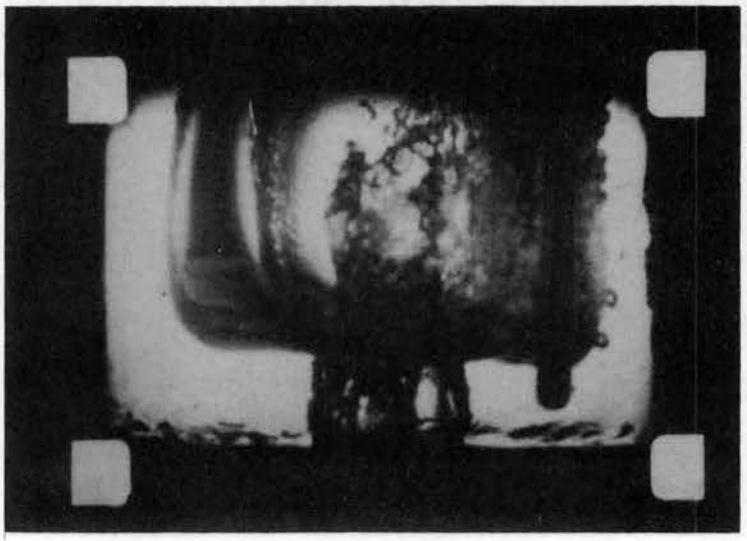

(b)

Figure 26. Turbulent Stream of Fluid Droplets

Examination of motion pictures of other bubbles revealed a similar stem-imploding phenomenon. Since lift-off had not occurred, there must be another explanation for the minor temperature disturbances.

It is difficult to ascertain exactly what took place in the bubble stem during the implosion that might have caused the minor temperature excursions at the base of the stem. The author is of the opinion that the minor drops were merely one phase of a progressive series of events, the first of which was a sealing off of the bubble stem next to the bubble bottom.

After the stem sealed off, evaporation around the torus at the liquid-solid-vapor interface still continued. Since the vapor could no longer flow up the neck into the bubble interior, stem enlargement and an increase of pressure within the stem resulted. Soon, the pressure inside the stem was large enough to overcome the pressure inside the bubble as well as the surface tension forces where the stem was attached to the bubble bottom; the bottom then blew out of the bubble as the neck emptied into the bubble interior. Fluid was apparently carried along with the vapor since a stream of droplets was clearly visible in the bubble interior. The origin of the fluid droplets is still open to question. Since the bulk fluid was superheated, condensation on the stem or bubble walls does not seem likely. The droplets could be portions of the bubble bottom that shattered and were carried along with the vapor. They might also have originated in the fluid at the triple interface. Since the droplets were carried into the bubble interior in a stream rather than a temporary spray, the triple-interface origin seems more likely than an origin from shattered pieces of the bubble bottom. If the droplets did originate at the interfacial region, it

seems plausible that a large enough disturbance could have occurred at the base of the stem to cause fluid counterflow from the outer to inner radii. An immediate evaporation of the counterflowing fluid could have accounted for the minor temperature fluctuations recorded during the implosion. This concept, which is partly supported by supposition, is illustrated in Figure 27. Even this hypothesized model is contradicted by the minor drop at thermistor 6. At thermistor 6, the minor drop occurred before the thermistor was inside the bubble stem.

Although the above theory concerning the minor temperature disturbances contains suppositions and does not explain the happenings at thermistor 6, one thing is certain: The bubble had not left the surface at the time the minor disturbances took place. In fact, lift-off did not occur until almost the maximum time shown in Figure 20.

Another discrepancy associated with the motion of the contact radius concerns the evaporation to dryness at thermistor 8. The temperature-time curve for thermistor 8 indicates that evaporation to dryness had occurred, as a sharp temperature reversal took place at 78 msec. However, the plot of contact radius clearly shows that thermistor 8 was flooded by bulk fluid at approximately 63 msec. The surprising thing about the flooding of 8 is that no discontinuity occurred in the temperature-time trace at 63 msec. Evidentally heat continued to flow to the bubble interior at this location even after the location was covered with bulk fluid. These discrepancies at thermistor 8 also cast uncertainty on what actually took place at thermistor 7. When the dry radius information was plotted in Figure 25, the assumption was made that evaporation to dryness was possible at thermistor 7, but not at thermistor 8. The initial thickness profile in Figure 24 was

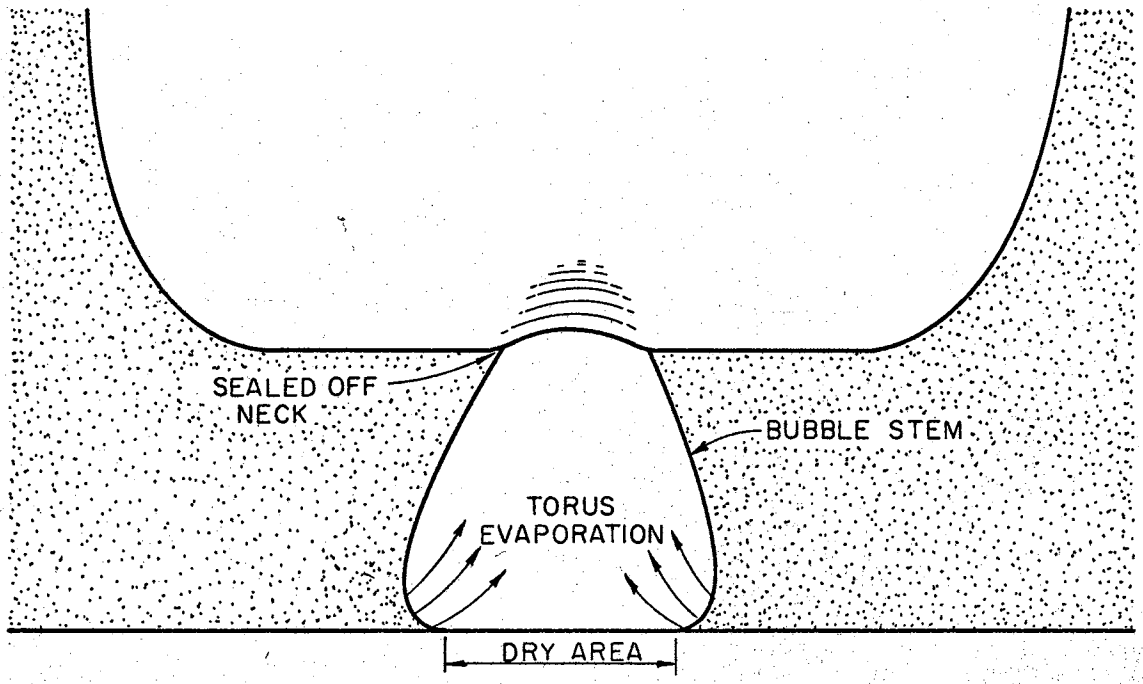

(a) BUBBLE STEM BEFORE IMPLOSION

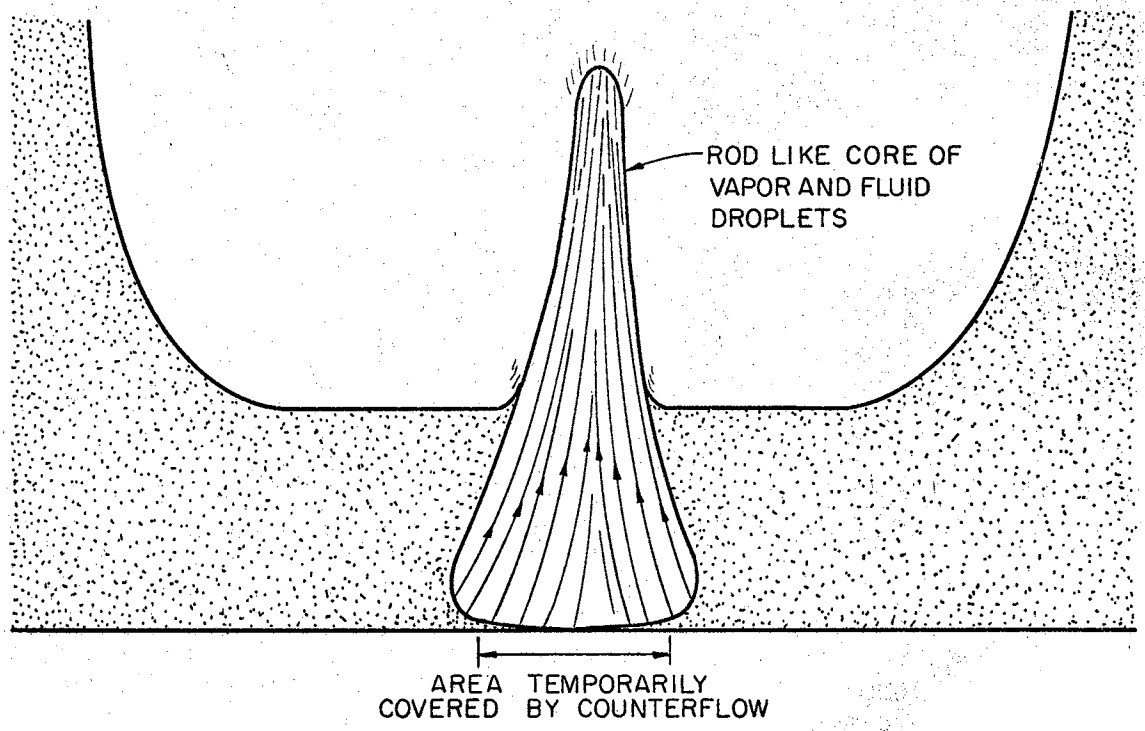

(b) BUBBLE STEM AFTER IMPLOSION

Figure 27. Hypothetical Model for Fluid Counterflow

extrapolated from thermistor 7 to thermistor 8 by using the technique illustrated in Figure 14. This made possible the evaluation of the δ values at thermistor 8 where evaporation to dryness was assumed impossible.

The above concepts raise an interesting question: Is the sharp reversal that occurs between Stage 1 and Stage 2 of Figure 14 definite proof of evaporation to dryness or does evaporation to dryness occur only at thermistors whose temperature trace contains both a major and a minor excursion. The investigators in [4] and [5] were of the opinion that the sharp reversal between Stage 1 and Stage 2 did indicate evaporation to dryness.

Much of the inconsistency or nebulosity associated with either evaporation to dryness or the minor temperature drops arose in the comparison of the position of the contact radius with thermistor location. In this investigation during the latter stages of growth, the contact radii measurements were plagued by two problems:

1. The line of sight between the camera and bubble was partly obstructed by adhesive between the boiler walls and the boiler plate.
2. The bubble moved from its position of symmetry with respect to the nucleating thermistor.

The accuracy of all of the contact radius measurements hinged on the assumption that the bubble grew with symmetry about the nucleation site. This assumption was necessary to relate bubble position to thermistor location as the line of sight of the camera was down the line of fifteen thermistors. However, during late growth stages, the interaction between the large bubble and the precision thermometer,

located in one corner of the boiler (Figure 26), caused the bubble to be drawn away slightly from its position of symmetry toward the thermometer. This motion undoubtedly led to error in measuring the contact radii.

The experimental conditions for this investigation were considerably different from those of previous investigators. Much larger bubbles were grown in a fluid that has not been reported and under superheated rather than saturated or subcooled conditions. However, it is still of interest to compare some of the microlayer information with that previously reported.

Katto and Yokoya [15] reported bubbles whose expanding dry radii conformed to equation (3-1). Although the expanding dry radius of Figure 25 is by no means a linear function of time, if a linear approximation is written for it, the slope is roughly 6200 compared to the 270 of [15]. Katto and Yokoya also reported that the velocity of the dry radius was much lower than the velocity of the bubble radius. If the slopes of the 'dry' and 'bubble' radii of Figure 24 are compared, they appear almost parallel except during the early, fast growth period. Since these slopes represent velocities, the velocity of the expanding dry radius and the bubble radius are comparable after the fast growth period.

A composite analytical and experimental equation for δ_i, equation (3-3), was also reported in [15]. For the initial microlayer profile of Figure 25, it is necessary to let the constant preceding the radical in (3-3) range from 2.3 to 3.4 to fit the data. Therefore, the microlayer profile of Figure 24 is not a strong function of the $\sqrt{r}$. Strong emphasis should not be placed on this comparison with the work of

Katto and Yokoya as the fluid in [15] was saturated water rather than superheated benzene. The bubbles were grown under dynamically constrained conditions and had maximum diameters of 0.4 in. compared to 2.35 in. for Figure 25.

When the shape of the instantaneous profiles of [14] and [17] were compared to those in Figure 24, a trend was noticed. In the two investigations where optical techniques were used to measure instantaneous thicknesses, the profiles were concave. In Figure 24 the concave trend is only exhibited for 2 msec and after this time the profiles are convex. The approximate slopes of the profiles in [14] and [17] were 12.7×10^{-2} and 6.7×10^{-4} respectively compared to 50×10^{-4} for Figure 24. Maximum bubble diameters were 0.4 in. and 0.75 in. respectively compared to 2.35 in. for Figure 24. The bubbles grown in [17] were heavily constrained as the height-to-diameter ratio was on the order of 1:3.

It was impossible in this investigation for the author to discern anything about the perimeter inflow described by Jawurek [14]. If such inflow took place, it probably happened at the larger radii where the microlayer formed and was immediately destroyed by the shrinking contact diameter before appreciable evaporation took place. The area of temporary microlayer existence is shown between thermistors 8 and 12 in Figure 24. Since the microlayer existed for only a short time in this region, the extrapolation from the 'dry' to the 'wet' region to extend the initial profile from thermistor 8 to thermistor 12, as illustrated in Figure 14, was not meaningful.

Cooper and Lloyd [5] coupled their experimental data to a simplified hydrodynamic model to arrive at (2-1). This equation does not

describe the δ_i profile of Figure 24, as the constant preceding the radical has to range from 0.51 to 0.66 to fit the data. Equation (2-1) also does not describe the data in Figure 6.

If bubble and contact radii were known as a function of time for a particular bubble, a crude analytical description of the formation and evaporation of the microlayer might be obtained by coupling (2-1) with the ideas illustrated in Figure 24, i.e.:

1. Microlayer formation is closely governed by the growth of the contact radius. Therefore, t_g might be approximated as the time for the contact radius to reach the point in question.
2. Substantial microlayer evaporation occurs between the bubble center and the maximum contact radii.
3. The velocity of the expanding dry radius is approximately equal to the radial velocity of the bubble after the fast growth period.
4. The slope of the instantaneous profiles is approximately equal to the slope of the initial profile.

Microlayer information should be obtained for many more bubbles under widely different conditions before the above concepts can be anything more than a very crude approximation used to describe the physical phenomena.

The above comparisons of present and past microlayer information indicate that there is still a great deal unknown. If any conclusions are to be drawn from the information in Figure 24 and Figure 25, the conclusions should be:

1. The propagation of the major temperature disturbance is more closely related to the motion of the contact radius than to the motion of the bubble radius.
2. The minor temperature excursions occur before the bubble has been torn from the heater surface. The minor excursion may possibly be the result of fluid counterflow in the bubble stem.
3. The microlayer evaporates to dryness in an expanding, wedge-like profile. The velocity of the dry radius is approximately equal to the radial velocity of the bubble after the fast growth period.

The author would like to stress that these conclusions should not be extrapolated to include smaller bubbles grown under drastically different conditions in other fluids.

This investigation in its entirety indicates that a great deal more experimental work needs to be done before microlayer evaporation can be fully understood. The number of individual investigations that could contribute to the literature is limited only by the imagination of the investigator. One experimental investigation that could clarify many of the existing mysteries of the microlayer might be performed with a composite of the apparatus used in this investigation and that used by Jawurek [14]. This composite would make possible the determination of microlayer thicknesses by two simultaneous independent approaches, one optical and the other heat transfer. Questions associated with perimeter inflow, stem counterflow and the convex versus concave instantaneous profile could be answered. If a suitable adhesive could be found to join the boiler sidewalls to the Electropane

boiler floor, the problem encountered in this investigation of adhesive obstruction in the line of sight during the contact diameter photography could be eliminated. However, it should be pointed out that the construction of just the boiler floor for such an investigation would be an extremely difficult undertaking. Until the method of vacuum deposition of thin film thermistors is developed to the state of being a science rather than an art, the undertaking of any microlayer investigation requiring elegant temperature measurements on the heat transfer surface will contiue to be a formidable task.

LIST OF REFERENCES

1. Applications Data for Kodak Photosensitive Resists. Kodak Publication No. P-91, Eastman Kodak Company, Rochester, New York.

2. Bankoff, S. G. "A Note on Latent Heat Transport in Nucleate Boiling." Journal of Amer. Inst. Chem. Engr., Vol. 8 (March, 1962), 63-65.

3. Bankoff, S. G., and J. P. Mason. "Heat Transfer From the Surface of a Steam Bubble in Turbulent Subcooled Liquid Stream." Journal of Amer. Inst. Chem. Engr., Vol. 8 (March, 1962), 30-33.

4. Cooper, M. G., and A. J. P. Lloyd. "Transient Local Flux in Nucleate Boiling." Proceedings of Third International Heat Transfer Conference, Chicago (1966), Vol. 3, 193-203.

5. _____. "The Microlayer in Nucleate Pool Boiling." Int. Journal of Heat and Mass Transfer, Vol. 12 (August, 1969), 895-913.

6. Fiock, E. F., D. C. Ginnings, and W. B. Holton. "Calorimetric Determination of Thermal Properties of Methyl Alcohol, Ethyl Alcohol, and Benzene." Journal of Research of the National Bureau of Standards, Vol. 6 (1931), 881-900.

7. Forster, Kurt, and R. Grief. "Heat Transfer to a Boiling Liquid--Mechanism and Correlations." Trans. of ASME, Series C, Journal of Heat Transfer, Vol. 81 (February, 1959), 43-53.

8. Graham, Robert W., and Robert C. Hendricks. "Assessment of Convection, Conduction, and Evaporation in Nucleate Boiling." National Aeronautics and Space Administration, TN D-3943, May, 1967.

9. Hendricks, Robert C., and Robert R. Sharp. "Initiation of Cooling Due to Bubble Growth on a Heating Surface." National Aeronautics and Space Administration, TN D-2990, April, 1964.

10. Hospeti, Narayan Bhimarao. "Investigation of Microlayer Vaporization Mechanism in Pool Boiling of Water at Atmospheric Pressure." Ph.D. Dissertation, University of Kansas, 1966.

11. Hospeti, Narayan B., and Russell B. Mesler. "Deposits Formed Beneath Bubbles During Nucleate Boiling of Radioactive Calcium Sulfate Solutions." Journal of Amer. Inst. Chem. Engr., Vol. 11 (July, 1965), 662-665.

12. International Critical Tables of Numerical Data, Physics, Chemistry and Technology. New York: McGraw-Hill Book Company, 1928.

13. Jacobs, J. D., and A. H. Shade. "Measurement of Temperatures Associated With Bubbles in Subcooled Pool Boiling." Presented at AIChE-ASME Heat Transfer Conference and Exhibit, Philadelphia, 1968.

14. Jawurek, H. H. "Simultaneous Determination of Microlayer Geometry and Bubble Growth in Nucleate Boiling." Int. Journal of Heat and Mass Transfer, Vol. 12 (August, 1969), 843-848.

15. Katto, Y., and S. Yokoya. "Experimental Study of Nucleate Boiling in Case of Making Interference-Plate Approach to the Heating Surface." Proceedings of Third International Heat Transfer Conference, Chicago (1966), Vol. 3, 219-227.

16. Kirby, D. B., and J. W. Westwater. "Bubble and Vapor Behavior on a Heated Horizontal Plate During Pool Boiling Near Burnout." Chemical Engineering Progress Symposium Series, Vol. 61 (1965), 238-248.

17. Madsen, N. "Temperature Fluctuations at a Heated Surface Supporting Pool Boiling of Water." Proceedings of the Institution of Mechanical Engineers, Vol. 180, Part 3C, 1965-1966, 150-159.

18. Manfield, H. G. "The Development of Thin Film Resistors and Capacitors for Microelectronics." Electronic Engineering, Vol. 35 (September, 1963), 588-594.

19. Maxwell, J. B. Data Book on Hydrocarbons. Princeton, New Jersey: D. Van Nostrand Company, Inc., 1950.

20. McSweeney, Thomas I. "Bubble Growth on a Glass Surface During Boiling of Ethyl Alcohol and Toluene." Ph.D. Dissertation, University of Michigan, 1967.

21. Moore, Franklin D., and Russell B. Mesler. "The Measurement of Rapid Surface Temperature Fluctuations During Nucleate Boiling of Water." Journal of Amer. Inst. Chem. Engr., Vol. 7 (December, 1961), 620-624.

22. Rogers, Thomas F., and Russell B. Mesler. "An Experimental Study of Surface Cooling by Bubbles During Nucleate Boiling of Water." Journal of Amer. Inst. Chem. Engr., Vol. 10 (September, 1964), 656-660.

23. Rohsenow, W. M., and J. A. Clark. "A Study of the Mechanism of Boiling Heat Transfer." Transactions of the ASME, Vol. 73 (July, 1951), 609-620.

24. Sharp, Robert R. "The Nature of Liquid Film Evaporating During Nucleate Boiling." National Aeronautics and Space Administration, TN D-1997, October, 1964.

25. Snyder, N. W. Summary of Conference on Bubble Dynamics and Boiling Heat Transfer Held at the Jet Propulsion Laboratory, June 14 and 15, 1956. S. G. Bankoff, W. J. Colahan, Jr., and D. R. Bartz, eds. Memo No. 20-137, Jet Propulsion Lab., California Institute of Technology, December 10, 1956, 13.

26. Snyder, N. W., and T. T. Robin. "Mass-Transfer Model in Subcooled Nucleate Boiling." Presented at AIChE-ASME Heat Transfer Conference and Exhibit, Philadelphia, 1968.

27. Thermophysical Properties Research Center Data Book. Nonmetallic Elements, Compounds and Mixtures, Vol. 2. Lafayette, Indiana: Perdue University.

28. Torikai, Kinichi. "Heat Transfer in a Contact Area of a Boiling Bubble on a Heating Surface." J.S.M.E. Bulletin, Vol. 10 (1967), 338-348.

29. Torikai, K., and T. Yamazaki. "Photographical Study of Boiling Heat Transfer Mechanism." Proceedings of Third International Heat Transfer Conference, Chicago (1966), Vol. 3, 239-244.

30. _____. "Dry State in a Contact Area of a Boiling Bubble on a Heating Surface." J.S.M.E. Bulletin, Vol. 10 (1967), 349-355.

31. Williams, J. D., and L. E. Terry. "Textural Electrical Properties of Vacuum-Deposited Germanium Films." Sandia Laboratory, Albuquerque, SC-R-67-1026, February, 1967.

32. Williams, J. D., L. E. Terry, and R. A. Settles. "Vacuum Deposited Germanium Films on Heated Amorphous Substrates." Sandia Laboratory, Albuquerque, SC-TM 306-63(14), November, 1963.

APPENDIXES

APPENDIX A

APPARATUS SPECIFICATIONS

Adhesive

G. E. RTV silicone rubber to bond boiler to thermistor plate.

Boiler

2 1/2 inches x 2 1/2 inches x 4 inches inside measurements, pyrex cell special ordered from Labglass Corporation.

Evaporation Boats

R. D. Mathis, S6-.010W and S21-.010W.

Heaters

Boiler and substrate, Thermolyne 8747-3F.

Molybdenum Foil

G. E. powder metallurgy, 0.002 inches thick x 6 inches wide.

Photography

Camera -- WF-4ST Fastax with Raptar f/2 lens.

Film -- Tri-X Reversal, type 7278, 16 mm.

Goose Controller -- WF-301.

Xenon Pulse Light -- Type 456 compact source.

Xenon Lamp Control Unit -- WF-360.

Potentiometer

Leeds and Northrup 8686.

Power Supplies

Harrison Lab 6266A, used for etching molybdenum foil.

Harrison Lab 865C, used to drive thermistor amplification circuit.

Recorder, Galvanometer

C. E. C. type 5-124

Galvanometers for data	7-320
Galvanometer for zero time	7-326
Grid Liner	158859
Internal Timer	15889
Paper	465124-5702
Take-up Reel	5-059
Trace Interrupter	158738

Recorder, Thermocouple

Leeds and Northrup Speedomax H.

Thermometer

Curtin 507446, 76 mm immersion, used in boiler.

Vacuum Station

VEECO VE-400 Evaporator Station, RG-3A Control Circuit.

APPENDIX B

THERMISTOR AND LEAD FABRICATION

The thermistors and their leads were fabricated using a process of vacuum deposition and photochemical milling on a piece of pyrex plate. The pyrex was cleaned and then coated by vacuum deposition with a copper alloy which was later etched to leave the desired lead configuration on glass. The active thermistor elements were then vacuum deposited through a mask onto the leads.

Vacuum Deposition

The vacuum deposition was done in a VEECO VE-400 vacuum station. The bell jar base plate had the following feed throughs:

1. Octal heater used to connect thermocouple and resistance monitor inside jar to read out devices outside jar.
2. Four evaporation source supply posts.
3. Two high-tension glow discharge posts.
4. Two substrate heater posts.
5. One push-pull rotary.

Figure 28 is a top view of the base plate showing the position of the various feed throughs.

The bell jar apparatus constructed for use with the VEECO system is illustrated in Figure 29. An aluminum structure supported a shutter mechanism, a substrate heater assembly and a pair of glow discharge

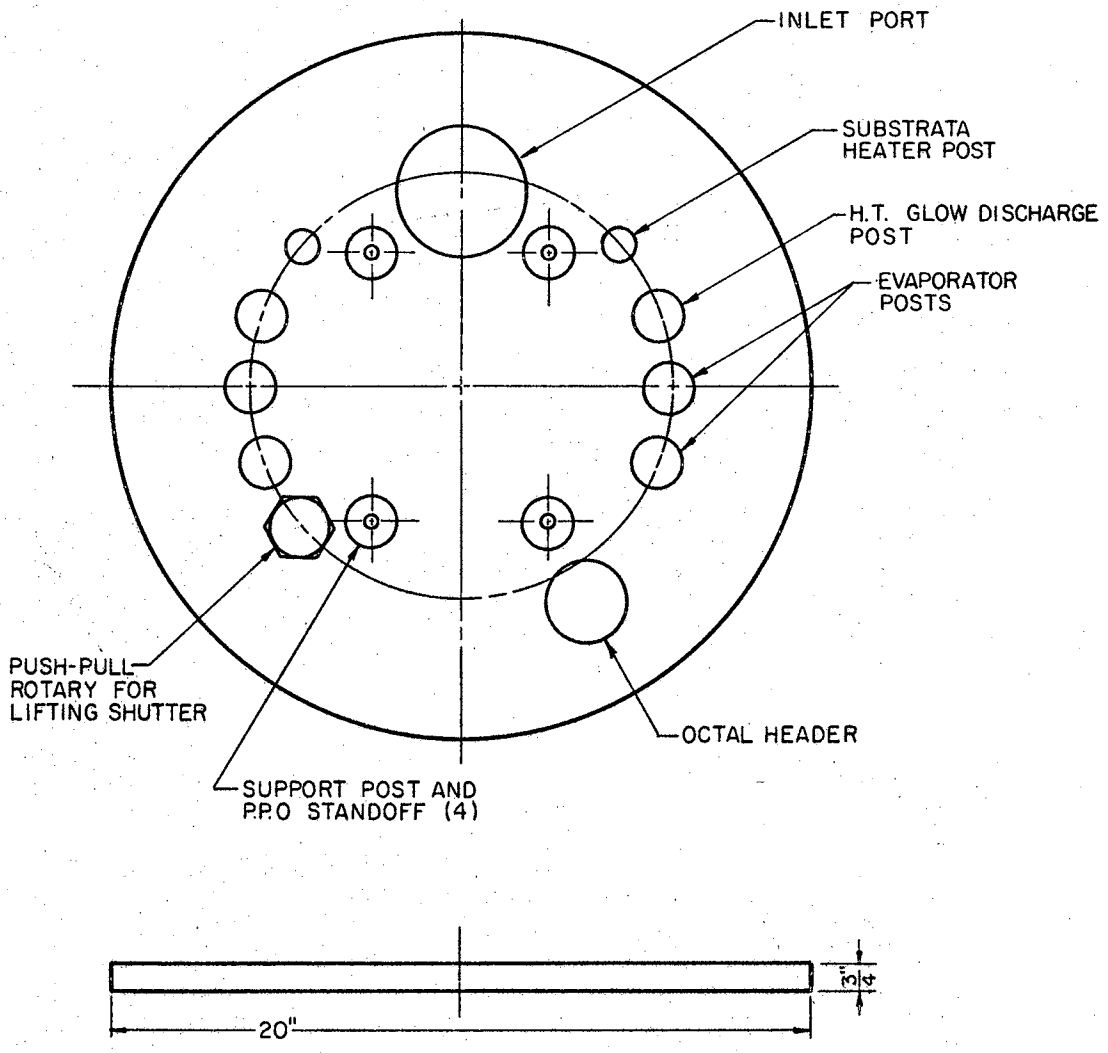

Figure 28. Top View of Baseplate

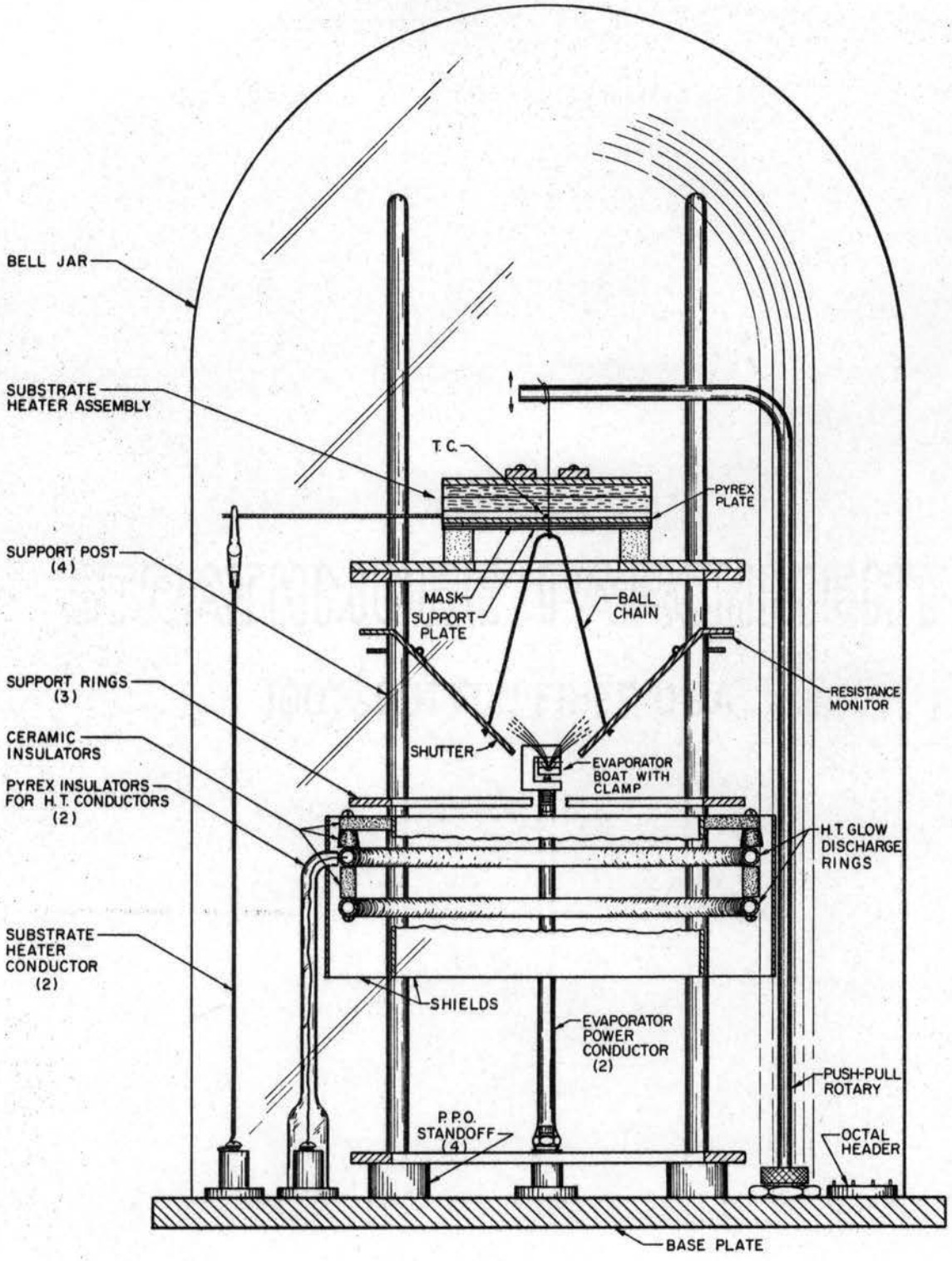

Figure 29. Vacuum Deposition Apparatus

rings. A resistance element clamped beneath the shutter monitored the inception of vaporization. The element was a microscope slide with a copper lead soldered at each end. Condensing metal bridged the gap between the leads and changed the resistance of the element.

In preparation for deposition of the lead material, the pyrex was cleaned by the process described in [31]. However, the glass was immersed in ethanol for storage following step (iv). Each piece was removed from the ethanol and given step (v) just prior to being loaded into the bell jar. In early trials adherence was improved by a final cleaning step performed inside the bell jar by electron bombardment from the high-tension glow discharge rings. However, with the change from pure copper to an alloy, the discharge cleaning was found unnecessary and was discarded.

After each piece of pyrex was dried in alcohol vapor, it was loaded in the substrate heater assembly illustrated in Figure 29. However, the molybdenum mask and mask support plate were removed for deposition of the lead metal. The assembly was placed in the bell jar where the pressure was reduced to 10^{-5} torr while the substrate was heated to 300°C. The lead metal [18] was then heated to inception of vaporization; at this instant, the boat current was slightly increased and the shutter was opened allowing the vapor stream to impinge upon the pyrex. When evaporation was complete, the shutter was closed and the bell jar was back filled to 10^{-2} torr with dry nitrogen. When the substrate had cooled to 50°C, the jar could be opened without oxidizing the freshly deposited film.

The substrate was removed from the jar and coated with photoresist. The resist was printed and then developed to leave behind a

protective film of polymerized resist in the image of the required lead configuration [1]. A micropositive of the lead configuration, shown in Figure 30, was produced by photographing a large drawing with seven-to-one reduction. After the resist was developed, the unprotected areas of metal film were etched away in ferric chloride to leave behind the thermistor leads. The protective coating of polymerized resist covering the leads was then removed with M-15 Dynachem Stripper. Step (v) of the cleaning process was repeated and the substrate was again loaded in the substrate heater assembly. This time the molybdenum mask

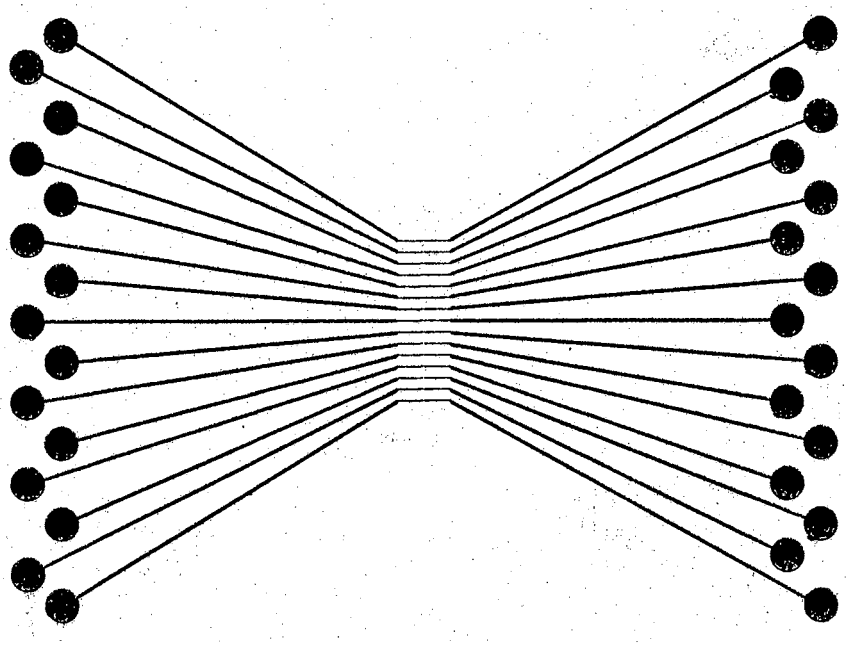

Figure 30. Lead Configuration (Actual Size)

and mask support plate were included in the sandwich. Special care was necessary to make sure that the holes in the molybdenum mask were in registration with the gap between each pair of thermistor leads. The heater assembly was then returned to the bell jar for deposition of the thermistor elements.

The pressure was again reduced to 10^{-5} torr inside the jar while the substrate was heated to 400°C to obtain a resistivity of five ohm-cm in the condensed germanium film [32]. The shutter was again used to protect the substrate during melting and outgassing of the germanium charge. The molybdenum mask used to deposit the thermistors was made by a photochemical milling process.

Mask Preparation

The molybdenum mask through which the thermistors were deposited was made from a piece of two mil foil. The foil was cleaned as described in [1] and then coated on both sides with KPR photoresist by the withdrawal method. The apparatus designed for the resist application is shown in Figure 31. The resist tank is stainless steel. A withdrawal rate of two inches per minute proved satisfactory. After application of the resist, the foil was given a 100°F, two-hour prebake and was wrapped in aluminum foil for lightproof storage. Storage of several months prior to printing the coated foil posed no problems.

The coated molybdenum foil was contact printed by placing it between two coincidentally aligned micropositives that were mirror images of each other. The micropositives were contact prints made from the negative produced by photographing a large drawing with seven-to-one reduction. The foil was printed one side at a time in a vacuum

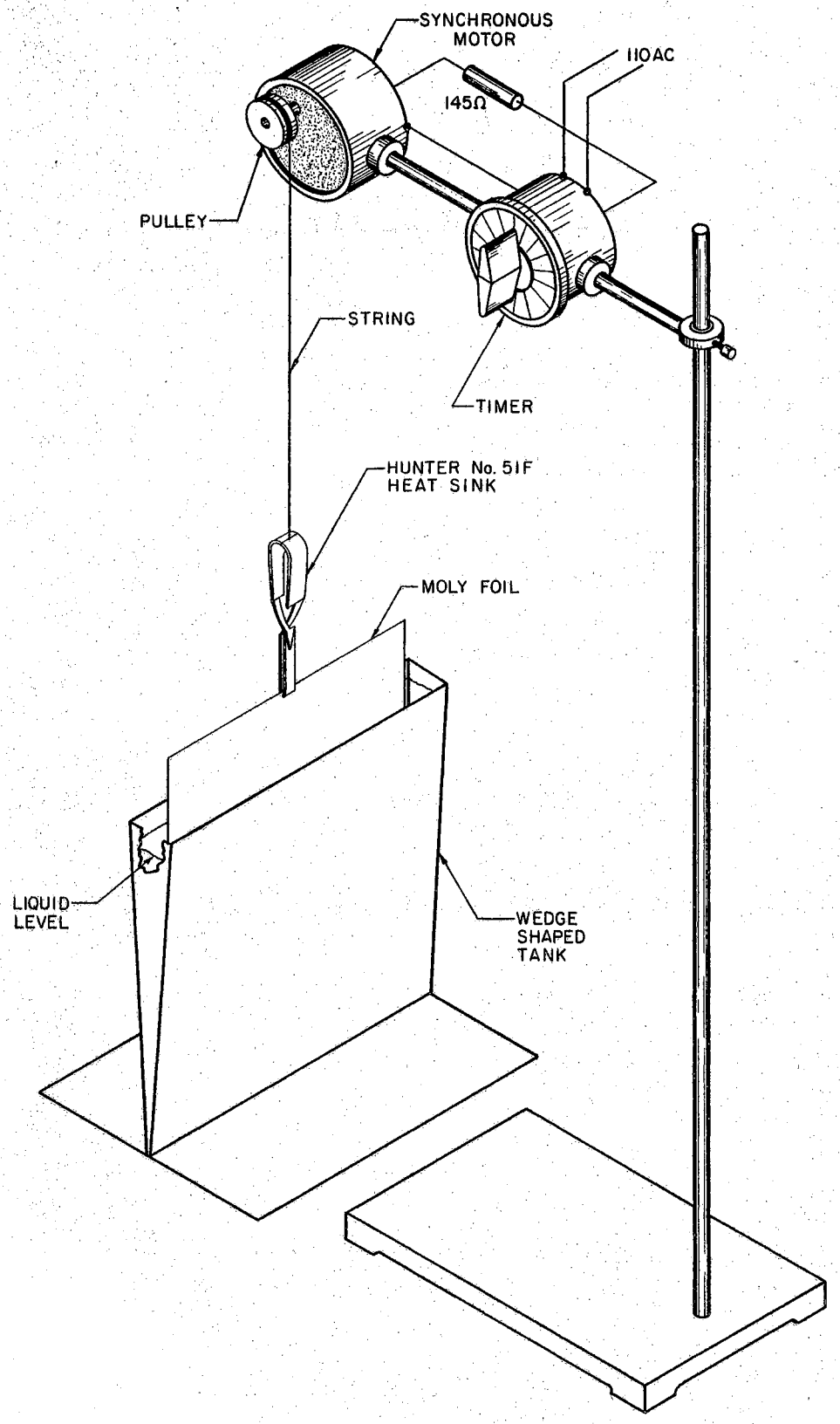

Figure 31. Apparatus for Photoresist Application

copy holder with carbon arcs whose intensity was 3000 foot candles measured at the copy board. Exposure time was two minutes.

Printing was followed by immersion for two minutes in KPR developer. The foil was removed from the developer and given a triple-pass spraying on both sides with technical grade xylene. A twenty-minute postbake at 450°F prepared the foil for the etch.

The foil was electrolytically etched in a 20 percent solution of sodium hydroxide, Figure 32. After a preliminary etch of 100 mA for one minute, the resist was checked for pin holes. These pin holes were

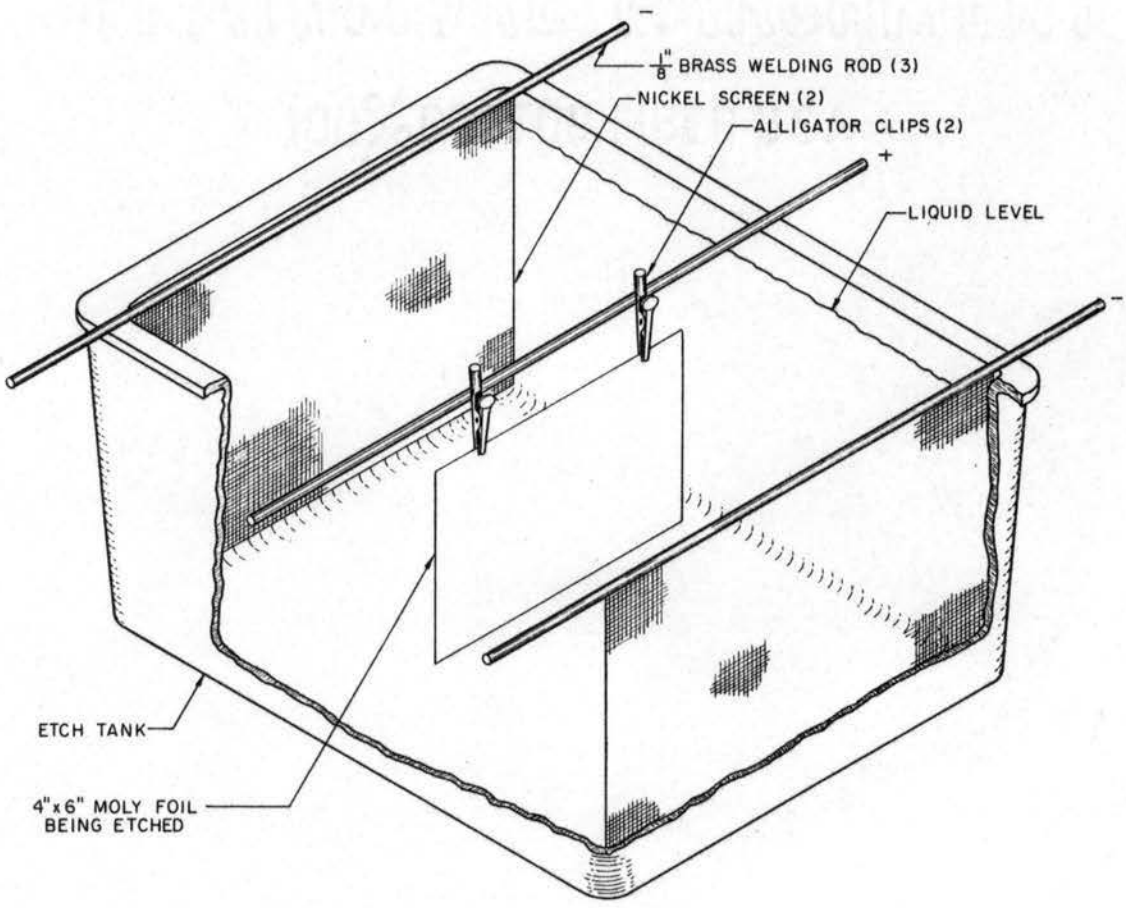

Figure 32. Tank for Electrolytic Etch of Mask

touched up and the foil was then given two etch steps of four minutes duration at 200 mA. A final step of one minute at 300 mA current completed etching.

After the etching, the photoresist was removed from the foil by immersing it in a solution of two parts HAS-27A to one part HAS-27B stripper manufactured by the Dynachem Corporation. The twenty-second immersion was followed by a tap water rinse with an aerator. The final cleaning described in [31], with steps (iii) and (vi) omitted, prepared the foil for use as a mask in the bell jar. The entire mask preparation process is illustrated in Figure 33. The holes etched were four mil by eight mil. Since the gap between thermistor lead pairs was four mil, the eight mil length of the holes etched in the mask gave the leads and thermistors a two mil overlap at each end to assure good ohmic contact.

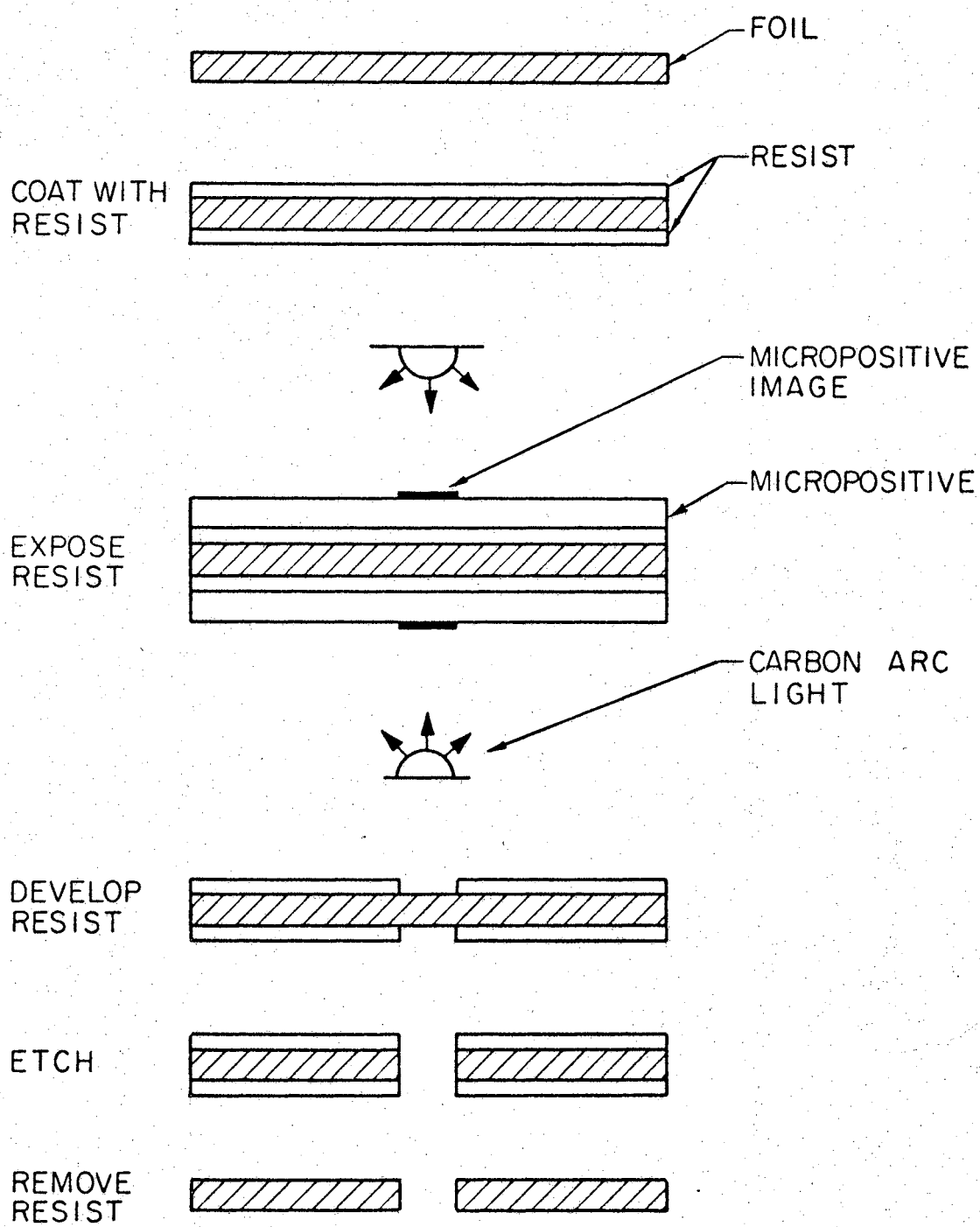

Figure 33. Steps in Mask Preparation

APPENDIX C

COMPUTER PROGRAM LISTINGS

```
C       HEAT TRANSFER PROGRAM                                                  100100
        DIMENSION TEMP(14),TMPO(43,53),TMPN(43,53),CAP(43,53),                 100110
       1 CONU(43,53),COND(43,53),CONL(43,53),CONR(43,53),HFLUX(53)             100120
1       FORMAT(F 7.1,I2,F6.0,F6.0,I2,I2)                                       100130
2       FORMAT(I2,3X,I3,2X,F10.3)                                              100140
20      FORMAT(8H1TIME = ,E14.7,70X,4HRUN ,I3,5X,5HPAGE ,I4)                   100150
21      FORMAT(1HO,12X,1H1,8X,1H2,8X,1H3,10X,2H10,7X,2H11,7X,2H12,             100160
       110X,2H29,7X,2H30,7X,2H31,10X,2H41,7X,2H42,7X,2H43)                     100170
22      FORMAT(2HO ,I4,1X,3F9.3,3X,3F9.3,3X,3F9.3,3X,3F9.3)                    100180
23      FORMAT(1H1,132X)                                                       100190
24      FORMAT(10HOHEAT FLUX)                                                  100200
25      FORMAT(4HO    ,I4,4X,7F17.0)                                           100210
30      READ(5,1) TMAX,NTH,TCR,TOL,NPRT,NRUN                                   100220
C       INITIALIZATION                                                         100230
        NC1 = 0                                                                100240
        NC2 = 0                                                                100250
        Z1 = .000005                                                           100260
        Z2 = .00005                                                            100270
        Z3 = .0005                                                             100280
        Z4 =(.000005 + .00005) / 2.                                            100290
        Z5 =(.00005 + .0005) / 2.                                              100300
        TINC = 0.2777777E-06                                                   100310
        STOL = TOL                                                             100320
        TIME = 0.0                                                             100330
        NON = 7                                                                100340
        NONTC = 41                                                             100350
        NDZ = NONTC + 2                                                        100360
        NDMX = (NTH - 1) * NON + NTH                                           100370
        RDIST = .000625                                                        100380
        ANGLE = .05                                                            100390
        DEN = 172.3                                                            100400
        TCG = .5927                                                            100410
        NTOT = NDMX * NONTC                                                    100420
        IPRT = 0                                                               100430
        NPG = 0                                                                100440
        STEP = 0.0                                                             100450
90      TOL = STOL                                                             100460
        NTOL = 0                                                               100470
        DO 100 I=1,NTH                                                         100480
100     READ(5,2) K,L,TEMP(K)                                                  100490
C       INTERPOLATE BETWEEN THERMISTORS                                        100500
200     NDN = 0                                                                100510
        J = NTH - 1                                                            100520
        SPC = NON + 1                                                          100530
        DO 220 IT=1,J                                                          100540
        NDN = NDN + 1                                                          100550
        TMPO(1,NDN) = TEMP(IT)                                                 100560
        DO 210 I=1,NON                                                         100570
        II = IT                                                                100580
        X = I                                                                  100590
```

```
      NDN = NDN + 1                                                    100600
210   TMPO(1,NDN)=TEMP(IT) - (X/SPC*(TEMP(IT)- TEMP(IT+1)))           100610
220   CONTINUE                                                         100620
      NDN = NDN + 1                                                    100630
      IT = II                                                          100640
      TMPO(1,NDN) = TEMP(IT+1)                                         100650
C     INTERPOLATE FOR FIRST ESTIMATE OF NODE TEMPERATURES              100660
300   IF(NC1.EQ.1) GO TO 400                                           100670
      NC1 = 1                                                          100680
      DO 320 J=1,NDMX                                                  100690
      TMPO(NDZ,J) = TCR                                                100700
      SPC = 1500.0                                                     100710
      N = 0                                                            100720
      DO 310 I=1,NONTC                                                 100730
      IF(I.GT.10) N = N + 9                                            100740
      IF(I.GT.29) N = N + 90                                           100750
      X = I + N                                                        100760
310   TMPO(I+1,J) = TMPO(1,J) - (X/SPC * (TMPO(1,J) - TMPO(NDZ,J)))    100770
320   CONTINUE                                                         100780
C     MOVE TMPO TO TMPN                                                100790
400   JJ = NONTC + 2                                                   100800
      DO 420 J=1,NDMX                                                  100810
      DO 410 I=1,JJ                                                    100820
410   TMPN(I,J) = TMPO(I,J)                                            100830
420   CONTINUE                                                         100840
C     CALCULATE CON AND CAP AT TIME ZERO                               100850
500   IF(NC2.EQ.1) GO TO 600                                           100860
      NC2 = 1                                                          100870
      DO 540 I=1,NDZ                                                   100880
      IF(I.LT.11) GO TO 504                                            100890
      IF(I.EQ.11) GO TO 501                                            100900
      IF((I.LT.30).AND.(I.GT.11)) GO TO 502                            100910
      IF(I.EQ.30) GO TO 503                                            100920
      IF(I.GT.30) ZDIST = Z3                                           100930
      GO TO 505                                                        100940
501   ZDIST = Z4                                                       100950
      ZDISU = Z1                                                       100960
      ZDISD = Z2                                                       100970
      GO TO 506                                                        100980
502   ZDIST = Z2                                                       100990
      GO TO 505                                                        101000
503   ZDIST = Z5                                                       101010
      ZDISU = Z2                                                       101020
      ZDISD = Z3                                                       101030
      GO TO 506                                                        101040
504   ZDIST = Z1                                                       101050
505   ZDISU = ZDIST                                                    101060
      ZDISD = ZDIST                                                    101070
506   DO 540 J=1,NDMX                                                  101080
      CONU(I,J) = 0.0                                                  101090
      COND(I,J) = 0.0                                                  101100
      CONL(I,J) = 0.0                                                  101110
      CONR(I,J) = 0.0                                                  101120
      CAP(I,J) = 0.0                                                   101130
      XX = J                                                           101140
      BR = (XX - .5) * RDIST                                           101150
      SR = (XX - 1.5) * RDIST                                          101160
      SH = .0001037037 * TMPO(I,J) + .1540252                          101170
      IF(J.EQ.1) SR = 0.0                                              101180
      IF(I.LT.NDZ) COND(I,J) = (TCG*((BR*BR)-(SR*SR))*ANGLE)/(ZDISD*2.) 101190
      IF(I.GT.1)   CONU(I,J) = (TCG*((BR*BR)-(SR*SR))*ANGLE)/(ZDISU*2.) 101200
      IF((I.EQ.1).OR.(I.EQ.NDZ)) GO TO 510                             101210
      IF(J.GT.1) CONL(I,J) = (TCG * SR * ANGLE * ZDIST) / RDIST        101220
      IF(J.LT.NDMX) CONR(I,J) = (TCG * BR * ANGLE * ZDIST) / RDIST     101230
      CAP(I,J) = (SH*DEN*((BR*BR)-(SR*SR))* ANGLE * ZDIST) / 2.        101240
      GO TO 540                                                        101250
510   IF(J.GT.1) CONL(I,J) = (TCG * SR * ANGLE * ZDIST) / (RDIST*2.)   101260
      IF(J.LT.NDMX) CONR(I,J) = (TCG * BR * ANGLE * ZDIST) / (RDIST*2.) 101270
      CAP(I,J) = (SH*DEN*((BR*BR)-(SR*SR))* ANGLE * ZDIST) / 4.        101280
540   CONTINUE                                                         101290
```

```
C     TEMPERATURE ITERATION                                                    101300
C        CALCULATION OF ERROR                                                  101310
600   INDEX = 0                                                                101320
      JJ = NDZ - 1                                                             101330
      DO 620 I=2,JJ                                                            101340
      DO 620 J=1,NDMX                                                          101350
      CONSM    =   CONU(I,J) + COND(I,J) + CONL(I,J) + CONR(I,J)               101360
      WORK = CAP(I,J) + TINC * CONSM                                           101370
      COEF1 = CAP(I,J)/WORK                                                    101380
      COEF2 = TINC / WORK                                                      101390
      SUMKT = 0.0                                                              101400
      IF(I.GT.1) SUMKT = SUMKT + TMPN(I-1,J) * CONU(I,J)                       101410
      IF(I.LT.NDZ) SUMKT = SUMKT + TMPN(I+1,J) * COND(I,J)                     101420
      IF(J.GT.1) SUMKT = SUMKT + TMPN(I,J-1) * CONL(I,J)                       101430
      IF(J.LT.NDMX) SUMKT = SUMKT + TMPN(I,J+1) * CONR(I,J)                    101440
      WORK = COEF1 * TMPO(I,J) + COEF2 * SUMKT                                 101450
      ERR = ABS(TMPN(I,J)  - WORK)                                             101460
      ERR = ERR/WORK                                                           101470
      IF(ERR.GT.TOL) GO TO 610                                                 101480
      INDEX = INDEX + 1                                                        101490
610   TMPN(I,J) = WORK                                                         101500
620   CONTINUE                                                                 101510
      IF(INDEX.LT.NTOT) GO TO 600                                              101520
      IF(NTOL) 630,630,700                                                     101530
630   TOL = TOL/10.                                                            101540
      NTOL = 1                                                                 101550
      GO TO 600                                                                101560
C     MOVE TMPN TO TMPO                                                        101570
700   DO 720 J=1,NDMX                                                          101580
      DO 710 I=1,NDZ                                                           101590
710   TMPO(I,J) = TMPN(I,J)                                                    101600
720   CONTINUE                                                                 101610
      IF(STEP.GE.TMAX) GO TO 810                                               101620
      IPRT = IPRT + 1                                                          101630
      IF(IPRT.EQ.NPRT) GO TO 800                                               101640
      GO TO 900                                                                101650
800   IPRT = 0                                                                 101660
810   LNCT = 29                                                                101670
      DO 840 J = 1,NDMX                                                        101680
      IF(LNCT-29) 830,820,820                                                  101690
820   NPG = NPG + 1                                                            101700
      WRITE(6,20) TIME,NRUN,NPG                                                101710
      WRITE(6,21)                                                              101720
      LNCT = 0                                                                 101730
830   LNCT = LNCT + 1                                                          101740
      WRITE(6,22)J,(TMPO(I,J),I=1,3),(TMPO(I,J),I=10,12),                      101750
     1(TMPO(I,J),I=29,31),(TMPO(I,J),I=41,43)                                  101760
840   CONTINUE                                                                 101770
900   NPG = NPG + 1                                                            101780
      WRITE(6,20) TIME,NRUN,NPG                                                101790
      WRITE(6,24)                                                              101800
      ZDIST = .000005                                                          101810
      DO 910 J=1,NDMX                                                          101820
910   HFLUX(J) = (TCG*(TMPN(2,J)-TMPN(1,J)))/ ZDIST                            101830
      K = (NDMX/7) * 7                                                         101840
      L = NDMX - K                                                             101850
      DO 920 I=1,K,7                                                           101860
      N = I + 6                                                                101870
      II = I                                                                   101880
920   WRITE(6,25) I,(HFLUX(J), J=I,N)                                          101890
      I = II                                                                   101900
      I = I + 7                                                                101910
      IF(L.GT.0)WRITE(6,25) I,(HFLUX(J), J=I,NDMX)                             101920
      STEP = STEP + 1.0                                                        101930
      TIME = STEP * TINC                                                       101940
      IF(TIME.LE.TMAX*TINC) GO TO 90                                           101950
      END                                                                      101960
```

```
C CALCULATION OF INITIAL AND INSTANTANEOUS MICROLAYER THICKNESS          100100
      DIMENSION HF(15),TP(15),C(15),DEN(15),HOV(15),TCM(15),SH(15)       100110
      DIMENSION TINT(15),ITME(100),FLNT(100),MTIME(100,15),TINST(100,15) 100120
      DIMENSION BSTAR(15)                                                100130
1     FORMAT (I2,I2,F6.0,I2,I1,F6.0,A4,A4)                               100140
2     FORMAT (F10.0,F10.0,E15.8)                                         100150
3     FORMAT (33H1     INITIAL MICROLAYER THICKNESS,70X,4HRUN ,I3)       100160
4     FORMAT (1HO,10X,14HTHERMISTOR NO.,5X,24HTHICKNESS IN MICROINCHES)  100170
5     FORMAT (1HO,16X,I2,14X,E14.7)                                      100180
6     FORMAT (I3,E15.8)                                                  100190
7     FORMAT (I3,E15.8)                                                  100200
8     FORMAT (39H1     INSTANTANEOUS MICROLAYER THICKNESS,53X,4HRUN ,I3, 100210
     1  5X,5HPAGE ,I3)                                                  100220
9     FORMAT(133HOTIME  . . . . . .                                      100230
     1. . . THERMISTOR NUMBER . . . . . .                               100240
     2. . . . . )                                                       100250
10    FORMAT ( 5H MSEC,7X,2H 1,14X,2H 2,14X,2H 3,14X,2H 4,14X,2H 5,14X,  100260
     12H 6,14X,2H 7,14X,2H 8)                                           100270
11    FORMAT (1H ,10X,A4,12X,A4,12X,A4,12X,A4,12X,A4,12X,A4,12X,A4,12X,  100280
     1A4)                                                               100290
12    FORMAT (1H ,I4,8E16.7)                                             100300
13    FORMAT ( 5H MSEC,7X,2H 9,14X,2H10,14X,2H11,14X,2H12,14X,2H13,14X,  100310
     12H14,14X,2H15)                                                    100320
14    FORMAT (1H ,10X,A4,12X,A4,12X,A4,12X,A4,12X,A4,12X,A4,12X,A4,12X,A4) 100330
15    FORMAT (1H ,I4,7E16.7)                                             100340
16    FORMAT(E14.7)                                                      100350
      READ(5,1) NT,NTI,TSAT,NRUN,NFLU,PTEMP,STAR,BLANK                   100360
      READ(5,2) (HF(I),TP(I),C(I), I=1,NT)                               100370
C CALCULATION OF CONSTANTS                                               100380
      DO 150 I=1,NT                                                      100390
      FAVTM = (TSAT + TP(I)) / 2.                                        100400
      CAVTM =  .5556 * (FAVTM-32.0)                                      100410
      AVTMK = CAVTM + 273.0                                              100420
      IF(NFLU.EQ.1) GO TO 100                                            100430
C TOLUENE                                                                100440
      DEN(I) = .88412 - .92248E-03*CAVTM + .0152E-06*(CAVTM*CAVTM)       100450
     1  - 4.223E-09*CAVTM**3                                             100460
      HOV(I) = 11637. - 4.823 * AVTMK - 1.26E-02 * (AVTMK*AVTMK)         100470
      HOV(I) = HOV(I) * (454./(92.134 * 252.))                           100480
      TCM(I) = 502.54 - .607275 * AVTMK                                  100490
      SH(I) = .451584 - 1.65686E-03*AVTMK + 7.12868E-06*(AVTMK*AVTMK)    100500
     1  - 6.82620E-09*AVTMK**3                                           100510
      GO TO 125                                                          100520
C BENZENE                                                                100530
100   DEN(I) = .90005 - 1.0636E-03*CAVTM - .0376E-06*(CAVTM*CAVTM)       100540
     1 - 4.223E-09*CAVTM**3                                              100550
      HOV(I) = 447.72 - .6163*CAVTM - 6.141E-04*(CAVTM*CAVTM)            100560
     1 - 1.509E-06*CAVTM**3                                              100570
      HOV(I) = HOV(I) / 2.32444                                          100580
      TCM(I) = 525.278 - 0.604093*AVTMK                                  100590
      SH(I) = .283708 + 2.75787E-04*AVTMK + 2.34387E-07*(AVTMK*AVTMK)    100600
     1 + 1.06981E-09*AVTMK**3                                            100610
125   DEN(I) = DEN(I) * 62.426                                           100620
      TCM(I) = TCM(I) * 2.419E-04                                        100630
150   CONTINUE                                                           100640
C CALCULATION OF INITIAL MICROLAYER THICKNESS                            100650
      WRITE(6,3) NRUN                                                    100660
      WRITE(6,4)                                                         100670
      DO 200 I=1,NTI                                                     100680
      A= (DEN(I)*SH(I)*HF(I)) /(2.*TCM(I))                               100690
      B = DEN(I)*(HOV(I)+(SH(I)*(TSAT-PTEMP)))                           100700
200   TINT(I) = (-B + SQRT(B*B - 4.*A*C(I)))/(2. * A)                    100710
      NTI = NTI + 1                                                      100720
      IF(NTI.LE.NT) READ(5,16) (TINT(I),I=NTI,NT)                        100730
      DO 250 I=1,NT                                                      100740
      WORK = TINT(I)*12.0E+06                                            100750
250   WRITE(6,5)I,WORK                                                   100760
C CALCULCATION OF INSTANTANEOUS MICROLAYER THICKNESS                     100770
C    ZERO OUTPUT AREA                                                    100780
      DO 300 J=1,NT                                                      100790
```

```
      DO 300 I=1,100                                                    100800
      MTIME(I,J) = 0                                                    100810
300   TINST(I,J) = 0.0                                                  100820
      DO 400 I=1,NT                                                     100830
      READ(5,6) K,FMIN                                                  100840
      READ(5,7) (ITME(J),FLNT(J), J=1,K)                                100850
      CONST = DEN(I) *((HOV(I) + SH(I)*(TSAT-PTEMP))                    100860
     1 + ((SH(I)*HF(I)*TINT(I)) / (2.*TCM(I))))                         100870
      DO 400 J=1,K                                                      100880
      L = ITME(J)                                                       100890
      MTIME(L,I)  = ITME(J)                                             100900
      TINST(L,I) = TINT(I) -((FLNT(J) - FMIN) / CONST)                  100910
400   TINST(L,I) = TINST(L,I)*12.0E+06                                  100920
C PRINT OUTPUT OF INSTANTANEOUS CALCULATION                             100930
      NPG = 0                                                           100940
      LNCT = 25                                                         100950
      L = 8                                                             100960
      IF(NT.LT.8) L = NT                                                100970
      DO 600 I=1,100                                                    100980
      DO 500 K=1,L                                                      100990
      BSTAR(K) = BLANK                                                  101000
500   IF(MTIME(I,K).EQ.0) BSTAR(K) = STAR                               101010
      IF(LNCT-25) 550,540,540                                           101020
540   NPG = NPG + 1                                                     101030
      WRITE(6,8) NRUN,NPG                                               101040
      WRITE(6,9)                                                        101050
      WRITE(6,10)                                                       101060
      LNCT = 0                                                          101070
550   LNCT = LNCT + 1                                                   101080
      WRITE(6,11) (BSTAR(K), K=1,L)                                     101090
600   WRITE(6,12) I,(TINST(I,K), K=1,L)                                 101100
      IF(NT.LE.8) GO TO 900                                             101110
      L = 15                                                            101120
      IF(NT.LT.15) L = NT                                               101130
      DO 800 I=1,100                                                    101140
      DO 700 K=9,L                                                      101150
      BSTAR(K) = BLANK                                                  101160
700   IF(MTIME(I,K).EQ.0) BSTAR(K) = STAR                               101170
      IF(LNCT-25) 750,740,740                                           101180
740   NPG = NPG + 1                                                     101190
      WRITE(6,8) NRUN,NPG                                               101200
      WRITE(6,9)                                                        101210
      WRITE(6,13)                                                       101220
      LNCT = 0                                                          101230
750   LNCT = LNCT + 1                                                   101240
      WRITE(6,14) (BSTAR(K), K=9,L)                                     101250
800   WRITE(6,15) I,(TINST(I,K), K=9,L)                                 101260
900   CONTINUE                                                          101270
      END                                                               101280
```

VITA

Harvey Parnell Metzler

Candidate for the Degree of

Doctor of Philosophy

Thesis: THE INVESTIGATION OF MICROLAYER GEOMETRY DURING NUCLEATE BOILING ON A FLAT PLATE

Major Field: Mechanical Engineering

Biographical:

Personal Data: Born in Colby, Kansas, October 8, 1940, the son of Clyde C. and Iva D. Metzler.

Education: Attended elementary school in Colby, Kansas, graduated from Colby Community High School in 1958; received the Associate of Arts degree from Independence Community College, Independence, Kansas, in May, 1960; received the Bachelor of Science degree from the University of Kansas, Lawrence, Kansas, with a major in Mechanical Engineering, in June, 1963; received the Master of Science degree from the University of Kansas, Lawrence, Kansas, with a major in Mechanical Engineering, in June, 1967; completed the requirements for the Doctor of Philosophy degree in May, 1970.

Professional Experience: Employed by the Mechanical Engineering Department at the University of Kansas, Lawrence, Kansas, as Graduate Assistant, September, 1962, to February, 1963, and September, 1963, to February, 1964; presently employed by Sandia Laboratories, Albuquerque, New Mexico, as Mechanical Engineer.

Professional Societies: Is a member of Pi Tau Sigma, Sigma Tau, and Tau Beta Pi.